

## Article

# Real Driving Cycle Simulation of a Hybrid Bus by Means of a Co-Simulation Tool for the Prediction of Performance and Emissions

Andrea Massimo Marinoni <sup>1,\*</sup> , Angelo Onorati <sup>1</sup> , Giacomo Manca Di Villahermosa <sup>2</sup> and Simon Langridge <sup>2</sup> 

<sup>1</sup> Politecnico di Milano, Department of Energy, Via Lambruschini 4A, 20156 Milano, Italy; angelo.onorati@polimi.it

<sup>2</sup> FPT Motorenforschung AG, 9320 Arbon, Switzerland; giacomo.manca-di-villahermosa@ivecogroup.com (G.M.D.V.); simon.langridge@ivecogroup.com (S.L.)

\* Correspondence: andreamassimo.marinoni@polimi.it

**Abstract:** This work is focused on the simulation of a complete hybrid bus vehicle model performing a real-world driving cycle. The simulation framework consists of a coupled co-simulation environment, where all the vehicle sub-system models are linked to achieve a real time exchange of input and output signals. In the vehicle model also the electric devices of the powertrain and accumulation system are included. This co-simulation platform is applied to investigate the hybridization of a 12-m city bus, performing a typical urban driving mission. A comparison between the conventional powertrain is performed against the hybridized version, to highlight the advantages and challenges. In particular, the novelty of this modeling approach is that the IC engine simulation does not rely on pre-processed look-up tables, but exploits a high-fidelity one-dimensional thermo-fluid dynamic model. However, it was necessary to develop a fast simulation methodology to exploit this predictive tool, achieving a low computational cost. The 1D engine model is first validated against the experimental engine map data available, showing a good model predictivity. Then the 1D engine model and the other models of the powertrain are coupled to the vehicle model, in order to follow the prescribed velocity profile of the driving cycle. The complete model is applied under different conditions, to evaluate the impact on performance and emissions and assess the simulation predictivity.

**Keywords:** hybrid diesel modeling; 1D co-simulation; fast simulation method; hybrid bus; driving cycle prediction; steady state map; 1D model validation



**Citation:** Marinoni, A.M.; Onorati, A.; Manca Di Villahermosa, G.; Langridge, S. Real Driving Cycle Simulation of a Hybrid Bus by Means of a Co-Simulation Tool for the Prediction of Performance and Emissions. *Energies* **2023**, *16*, 4736. <https://doi.org/10.3390/en16124736>

Academic Editor: Evangelos G. Giakoumis

Received: 26 April 2023

Revised: 5 June 2023

Accepted: 14 June 2023

Published: 15 June 2023



**Copyright:** © 2023 by the authors. Licensee MDPI, Basel, Switzerland. This article is an open access article distributed under the terms and conditions of the Creative Commons Attribution (CC BY) license (<https://creativecommons.org/licenses/by/4.0/>).

## 1. Introduction

Nowadays legislators are introducing increasingly stringent limits on internal combustion engines (ICE) to ensure the lowest tailpipe emissions. In this scenario, the latest Euro 7 regulation certainly represents a demanding task for the automotive industry. In particular, the attention is shifting towards a real-world verification of emissions, with a homologation process that considers the true conditions of vehicle use [1,2]. However, the increasing electrification of the powertrain, like the hybridization, on one hand has the potential of reducing fuel consumption and CO<sub>2</sub> emissions, while on the other hand poses additional challenges with regard to other pollutant emissions, such as nitrogen oxides [3,4]. For example, it is very important to predict the impact of multiple, long or short engine-off periods on the conversion efficiency of the after-treatment system. Hence, the capability to correctly predict the engine behavior under real driving conditions, typically by means of a digital twin of the production vehicle, is becoming more and more important [5].

More specifically, 1D thermo-fluid dynamic simulations of IC engines have been commonly employed during the last decades to investigate and optimize the performance and emissions [6]. In early works such as [7], the IC engine has been usually represented by a 0D look-up table map, to be coupled to other models representing the powertrain and

the vehicle. The low computational effort required by this approach has contributed to its widespread use. However, the IC engine is a volumetric machine, which, for example, cannot instantly respond to any torque request [8], due to the typical transient thermo-fluid dynamic phenomena occurring in the whole engine system. This is especially important for the vehicle longitudinal dynamics simulation. Later works highlighted the importance of using a transient 1D thermo-fluid dynamic model to correctly predict the IC engine emissions and performance under transient conditions [9].

When modelling a modern hybrid vehicle, many additional sub-systems have to be included, and this is often done by simulating each component as a standalone device, using the output of a model as input for the other. In this study a complete co-simulation methodology is described, to allow a real time interaction between the vehicle sub-models. A good example of how this approach can be exploited for the thermal management analysis is found in [10]. This framework avoids multiple iterative simulation loops, hence reducing the total development process.

Overall, the main innovative contributions described in this work are the following:

- The internal combustion engine is not represented by a simple look-up table, containing the values of performances and emissions at different operating points. A complete 0D/1D thermo-fluid dynamic model is used to build up a satisfactory virtual engine, which generally increases the confidence in the model's predictions, since the relevant unsteady phenomena are included in the simulation. This eventually leads to significant advantages, such as:
  - a. better prediction of engine response to torque request: a more reasonable trend is achieved, since torque gradients are smoothed, leading to a more realistic transient calculation, rather different from the immediate torque availability provided by the engine look-up table.
  - b. The co-simulation predictions are therefore more reliable, since its output is influenced by the inter-connected IC engine model.
  - c. Eventually, a better calibration of the vehicle system can be achieved by means of simulation, to quickly reach the emission compliance.
- A new numerical method is used and validated to allow a fast simulation by the 1D model: the fast simulation method (FSM). This methodology allows the reduction in the CPU/real time ratio by up to 85 %, allowing to tackle the most challenging task: the driving cycle simulations by means of 1D models. In this way, it is possible to use the high-fidelity 1D engine model instead of an engine map (look-up table), thanks to the relevant reduction of computational time.
- The co-simulation environment achieved affects each sub-model's behavior by the inter-connected sub-models. This enhances and exploits the predictivity of the IC engine 1D model. For example, the back pressure felt by the 1D engine model is computed by the after-treatment model, which is well suited to cope with this task. Conversely, a map-based engine model is not sensitive to a dynamically changing boundary condition, such as the exhaust backpressure.

This manuscript is divided into the following sections: after the introduction, Section 2 highlights the vehicle characteristics, describing the conventional and hybrid powertrain architectures. In the same section the methodology used to obtain the driving cycle mission profile is reported. Section 3 is dedicated to the modelling and validation of the IC engine under steady state conditions. In Section 4 the co-simulation framework is discussed, presenting the different sub-models involved in the co-simulation environment. In Section 5 the sub-models representing the various vehicle components, such as the transmission and vehicle dynamics, are described. Section 6 discusses the conventional powertrain co-simulation model, while in Section 7 the calculated results are reported, highlighting the effect of different ambient temperature on the predicted emissions. Finally, Section 8 describes the hybridized powertrain co-simulation, highlighting the effect of different ambient temperatures on the electrified powertrain.

The development of the several vehicles sub-models has been performed in the framework of the European Project Vision-xEV [11] and the sub-models used have been built and validated by academic or industrial partners, as acknowledged in this manuscript.

## 2. 12-m Heavy-Duty Bus Characteristics

The chosen vehicle is a 12-m heavy-duty urban bus, powered by a 210 kW, 6-cylinder turbo-diesel engine. Its main characteristics are reported in Figure 1.



**Figure 1.** 12 m Heavy-Duty urban bus and vehicle specifications.

Urban busses make perfect candidates for low voltage hybridization, thanks to the highly transient cycles they are usually subject to during their operational life, with a high number of start/stop events and braking opportunities [12]. On the other hand, even on pure ICE vehicles of this kind, the exhaust after-treatment thermal management can be critical in these conditions, due to the low average load of the engine and the long times spent at idling, which translate into low exhaust gas enthalpy and a struggle to keep the ATS above the light-off temperature. Improving fuel consumption, which further erodes the exhaust gas enthalpy, can have an adverse effect on the tailpipe emissions of the vehicle.

For this study, the choice was made to adopt a 48 V P1 hybrid architecture shown in Figure 2, which constitutes an optimum for this kind of vehicle in terms of the balance between fuel consumption reduction potential and capital costs, thus minimizing the total cost of ownership.

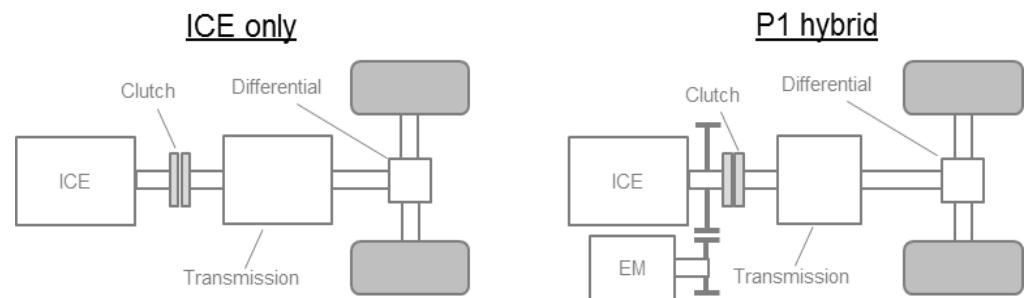


**Figure 2.** Scheme of the baseline vehicle and P1 configuration.

The choice of the mission is of paramount importance when defining the simulation setup: to obtain significant results, it should be consistent with the relevant homologation requirements and real-world working conditions of the vehicle. For this application the urban mission shown in Figure 3 has been chosen. The cycle is the "Urban" cycle proposed in VECTO [13].

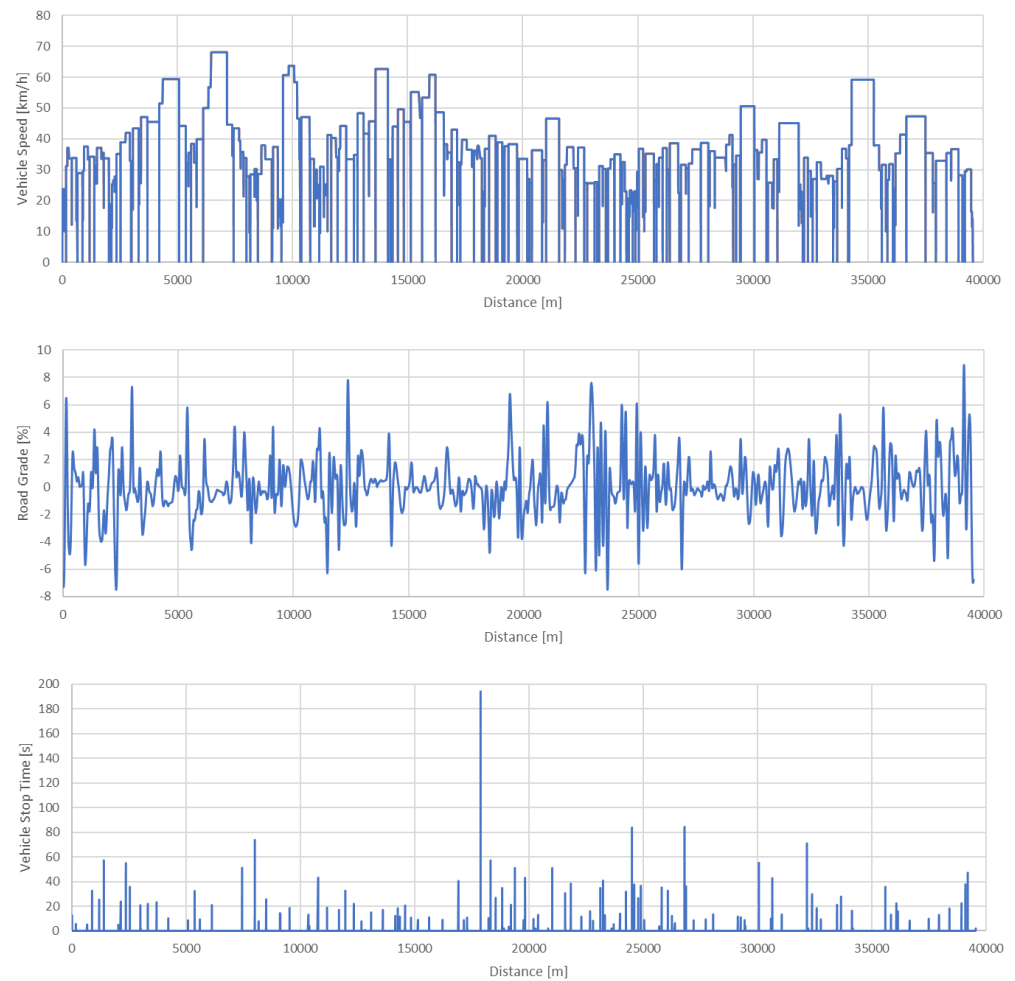


**Figure 3.** Mission speed target, road grade and vehicle stop times as a function of covered distance.

This mission speed target is defined as a function of the driven distance and has instantaneous velocity variations, which means that the actual speed profile will depend on each vehicle's performance and on the aggressiveness of the driver model. This choice was made so that the mission can be accomplished regardless of the performance of the vehicle.

To obtain a repeatable profile which does not depend on the powertrain configuration, the mission has been pre-processed using a simplified vehicle model, to generate a time-dependent speed profile shown in Figure 4.

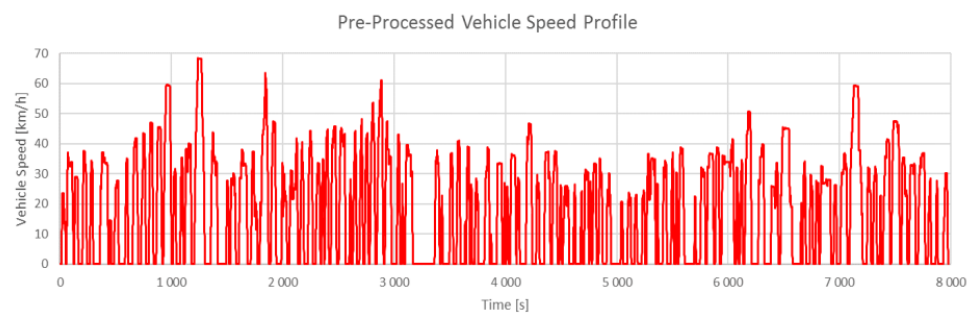


**Figure 4.** Pre-processed mission speed profile.

The simplified vehicle model is composed of a map-based engine, a transmission, a vehicle body and a driver, using VECTO-like rules [13] on overspeed, coasting to transform the target speed from distance based to time based. The coasting functionality allows

the vehicle to disconnect the engine from the driveline and proceed by inertia for a time interval, if the speed of the vehicle at the end of the coasting session does not deviate too much from the mission profile. Overspeed is activated when the vehicle approaches a slope by raising the target speed by a pre-defined value, to accumulate kinetic energy.

### 3. 1D Crank-Angle Resolved Thermos-Fluid Dynamic Engine Model

A complete 1D model has been built using the Gasdyn code [14,15] to predict performances and emissions of the 6.7L, 6-cylinder turbocharged heavy duty (HD) diesel engine, proposed as main propulsion system for the hybrid mid-size urban bus under consideration. The main engine geometrical data are presented in Table 1. The other engine parameters, such as valve lift profiles and flow coefficients, together with the turbocharger maps were available and provided by the manufacturer.

**Table 1.** Engine data.

Quantity	Value	Unit of Measure
Bore × Stroke	104 × 132	mm × mm
Rod length	195	mm
Number of cylinders	6	-
Compression ratio	16.8	-
Valves per cylinder	4	-
Fuel	Diesel	-

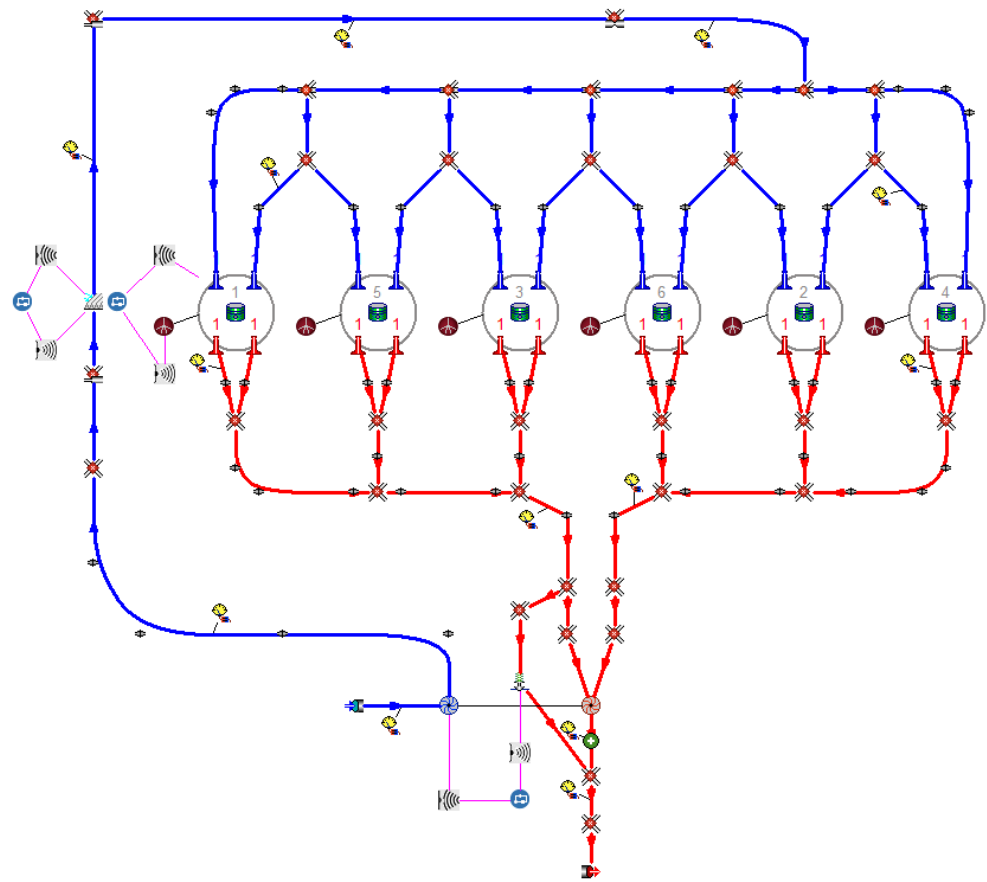
In particular, the 1D model consists of a detailed description of the entire intake and exhaust systems geometry and devices along the intake and exhaust lines [15]. The exhaust after-treatment system has not been included in the 1D model, modelled as an increased back-pressure imposed at the outlet boundary condition, according to the experimental measurements. A map-based approach for the simulation of turbine and compressor has been exploited [16]. The manufacturer turbocharger maps supplied had a limited number of mapped points and consisted of a small number of measured rotational speeds; hence, these maps have been extrapolated to cover a wider range of possible operating conditions [17]. In fact, the instantaneous mass flow rate through the turbocharge can vary due to the unsteady flow in the ducts. Regarding the fuel injection data, the complete map of the number of events, fuel rail pressure and start of injection (SOI) was available from the manufacturer.

The engine architecture features a wastegate valve to control the engine boost pressure, which affects only one side of the exhaust system, as depicted by the 1D schematic in Figure 5. To control the engine load, a proportional-integrative-derivative (PID) controller is used to achieve the target boost pressure and indicated torque, by controlling the wastegate opening and injected fuel mass (per cycle, per cylinder). The target boost pressure value has been imposed, according to the experimental measured pressure. Downstream of the compressor an intercooler is present to cool down the fresh charge.

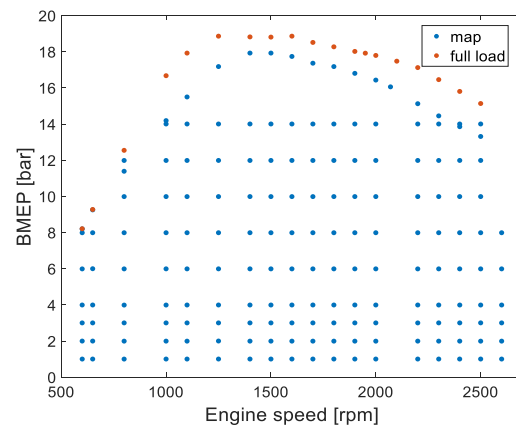
First of all, it is important to achieve a predictive model under steady state conditions, because during the driving cycle simulation the same 1D model is used, continuously varying the engine speed and load request, hence running the model across the whole range of operating conditions.

Figure 5 presents the 1D schematic of the 6-cylinder diesel engine, including the twin-entry, fixed geometry turbine with wastegate valve. It was important to build a detailed 1D schematic to correctly represent the twin-entry turbine in the exhaust system, as this configuration has a significant influence on the shape of pressure pulses and the energy available at the entry of the turbine.

Figure 6 shows the map of the experimentally investigated operating conditions used to perform the steady state validation of the 1D model. The 189 validation operating points are at constant engine speed and load, spread along the whole range of engine speeds and from low load to full load.



**Figure 5.** Complete 1D engine model (cylinder number 1–6).



**Figure 6.** Map of experimental points measured and validated (left); experimental test bench (right).

In the 1D thermo-fluid dynamic tool, the gas flow is assumed to be unsteady, compressible and one-dimensional [18]. The conservation laws of mass, energy and momentum are written as a non-linear hyperbolic system of partial differential equations, which is mathematically closed by adding the hypothesis on the properties of the working fluid. In this case the gas is assumed to be a perfect gas. Heat transfer and friction between the gas and the pipe walls are considered by dedicated source terms in the respective conservation equations, as described in [19,20].

Two numerical solvers have been exploited for the simulations in the 1D fluid dynamic code, depending on the application:

1. A robust, second order accurate, finite difference numerical scheme based on the Corberán–Gascón total variation diminishing (CG-TVD) method, for a detailed calculation on a refined mesh, which allows to smoothly capture the unsteady flows and waves occurring in the 1D domain [21,22].
2. A finite volume numerical solver for coarse meshes, to carry out a quick simulation: the fast simulation method (FSM). This is based on the “1D cell” method, which derives from the more general 3D cell method proposed in [23]. This finite volume method is based on the solution of the mass, energy and momentum conservation equations in time and is very conservative even with large mesh size, increasing the time step size and reducing the CPU/real time ratio. The method is explicit in time like the CG-TVD, while the main difference is that it is applied on a time-space staggered grid, evaluating quantities in the cell centers and fluxes in the ports, which are staggered by half time step and half mesh size [24]. Figure 7 shows the schematic of the numerical method.

The time step is always computed according to the Courant–Friedrichs–Lewy (CFL) criterion [25] to guarantee numerical stability. The boundary conditions connecting the 1D elements solution are resolved by a characteristic-based approach, to handle open ends, junctions, valves and the turbocharger, which is solved with a map-based approach [26].

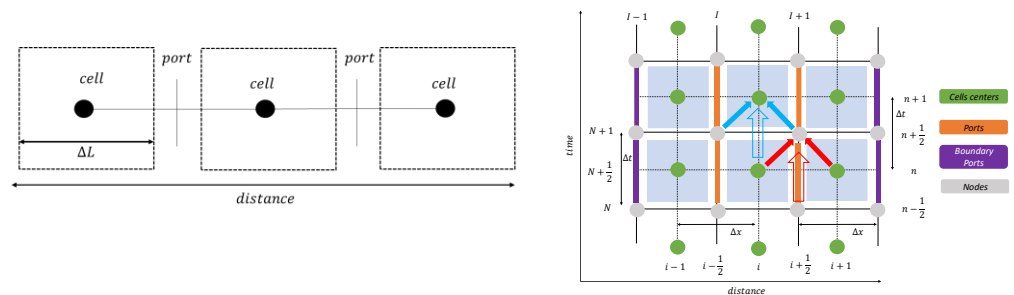


Figure 7. 1D cell domain discretization and time advancing staggered scheme.

The three differential conservation equations of mass, energy and momentum written in discrete form for the 1D cell method are reported below (Equations (1)–(3)):

$$\rho_{cell}^{t+1} = \rho_{cell}^t + \frac{\Delta t}{V_{cell}} \sum_P^{N_{ports}} (\rho u A)_{Ports}^{t+\frac{1}{2}} \quad (1)$$

$$(\rho e^0)_{cell}^{t+1} = (\rho e^0)_{cell}^t + \frac{\Delta t}{V_{cell}} \sum_P^{N_{ports}} (\rho u h^0 A)_{Ports}^{t+\frac{1}{2}} + S_e \quad (2)$$

$$(\rho u A)_{cell}^{t+\frac{1}{2}} = (\rho u A)_{cell}^{t-\frac{1}{2}} + \frac{\Delta t}{\Delta L_{cells}} \sum_P^{N_{ports}} [(p + \rho u^2) A]_{Ports} + S_m \quad (3)$$

In Equation (2),  $e^0$  is the specific total internal energy of the cell, and  $h^0$  is the specific total enthalpy of the cell. The perfect gas thermodynamics relationship holds, and the total energy  $e^0$  and enthalpy  $h^0$  are expressed as:

$$\begin{aligned} e_0 &= e + \frac{1}{2}u^2 \\ e &= c_v T \\ h_0 &= h + \frac{1}{2}u^2 \\ h &= e + RT = c_p T \end{aligned} \quad (4)$$

Moreover,  $u$  is the gas velocity,  $\rho$  is the gas density,  $A$  is the pipe section,  $p$  is the gas pressure and  $V$  is the cell volume.  $\Delta t$  and  $\Delta L$  are the time step size and the mesh size, respectively.  $S_e$  and  $S_e$  are the source terms of the corresponding equations, which take

account of heat transfer and friction at the duct walls. The symbol  $t$  indicates the time while the subscript *Ports* refers to the ports of the 1D cell method.

A brief description of the combustion model for the diesel engine is reported below. It has been developed [27] to handle current multi-pulse injection systems, ensuring fast run times. The 0D thermodynamic combustion model subdivides the chamber into three zones, as highlighted in Figure 8: fresh charge, fuel (vaporized) and burned gas, applying the first law of thermodynamics to evaluate the pressure and temperature variations.

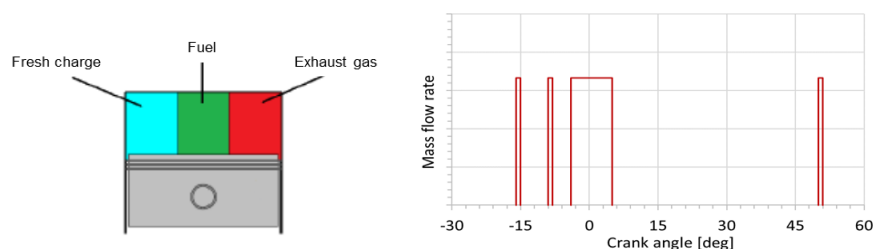


**Figure 8.** 0D schematic of the combustion chamber, split into three zones by the thermodynamic combustion model (left). Schematic of fuel mass injection into the cylinder by multiple events (right).

In this case the combustion rate is computed by means of multiple double-Wiebe laws [28,29], taking account of the in-cylinder conditions: pressure and temperature, gas composition (fresh charge, fuel and residuals) and injection timings. Each pulse injected during the compression/combustion phases burns with a rate defined by the following expression, as a function of the crank angle  $\theta$ :

$$x_b(\theta) = \beta \left( 1 - e^{-a_1 \cdot \left( \frac{\theta - \theta_{i,1}}{\theta_{f,1} - \theta_{i,1}} \right)^{m_1 + 1}} \right) + (1 - \beta) \cdot \left( 1 - e^{-a_2 \cdot \left( \frac{\theta - \theta_{i,2}}{\theta_{f,2} - \theta_{i,2}} \right)^{m_2 + 1}} \right) \quad (5)$$

where the first term into the brackets (1st Wiebe function) describes the premixed combustion phase, whereas the second term (2nd Wiebe function) describes the diffusive combustion phase. The coefficient  $\beta$  determines the dominating Wiebe function, while  $a_1$ ,  $a_2$ ,  $m_1$  and  $m_2$  are the typical coefficients of the Wiebe function. The angles  $\theta_{i,1}$ ,  $\theta_{i,2}$ ,  $\theta_{f,1}$  and  $\theta_{f,2}$  are the starting and final angles of the Wiebe function, calibrated for each simulated operating point according to the comparison with the experimental, instantaneous in-cylinder pressure. The results of this approach are presented in [14], where it is shown how this equation is able to describe the rate of burned mass fraction with respect to the experimental one.

The pollutant emission prediction relies on chemical equilibrium models and empirical correlations, as described in [30,31]. In particular, in this study where diesel combustion is involved, the main pollutant of interest is  $\text{NO}_x$ .

The result of the 1D model simulation, carried out on 189 engine operating points, is now presented. The experimental data have been normalized with respect to a constant value to preserve the trends. For each comparison the experimental and predicted values, the percentage difference and the absolute difference between experimental data and calculated results are reported.

Figure 9 shows the contour plots of the measured and computed brake-specific fuel consumption (BSFC in g/kWh), with the relative and absolute errors on the whole steady engine map. The agreement with the measured data is satisfactory and the trend is well captured. This is the most important validation to achieve a predictive model, which can be used for the simulation of a driving cycle with good confidence about the total fuel consumption.

In addition, Appendix A reports further results concerning the steady state validation of the 1D model. Figures A1 and A2 describe the calculated equivalence ratio and the air mass flow rate, showing a good agreement with measured data, with reasonable

discrepancies. The correct prediction of the mass flow rate is very important for the prediction of the pollutant emissions across the exhaust after-treatment system, since its conversion efficiency depends on the mass flow and temperature of the incoming exhaust gases from the cylinders.

Similarly, Figures A3 and A4 report the predicted gas temperature and pressure at the turbine inlet, showing a very good agreement with experimental measurements, with only a very small percentage error.

The virtual engine model demonstrated a high accuracy with regard to the in-cylinder peak pressure, reported in Figure A5, as well as to the turbocharger rotational speed, reported in Figure A6. This shows a good matching of the turbocharger model to the real turbomachine.

Finally, the calculated cylinder-out concentrations of NO<sub>x</sub> pollutant emission have been compared to the measured data on the whole engine map. Figure A7 highlights the contour maps and the percentage errors. The NO<sub>x</sub> prediction is fairly good, with an average error of around 10–20%, but with peak error of 150% in the region of high engine speeds and very low loads. However, this error occurs when the NO<sub>x</sub> concentration is very small. The in-cylinder experimental pressure data have been used to improve the calibration of the combustion model and the prediction of NO<sub>x</sub>.

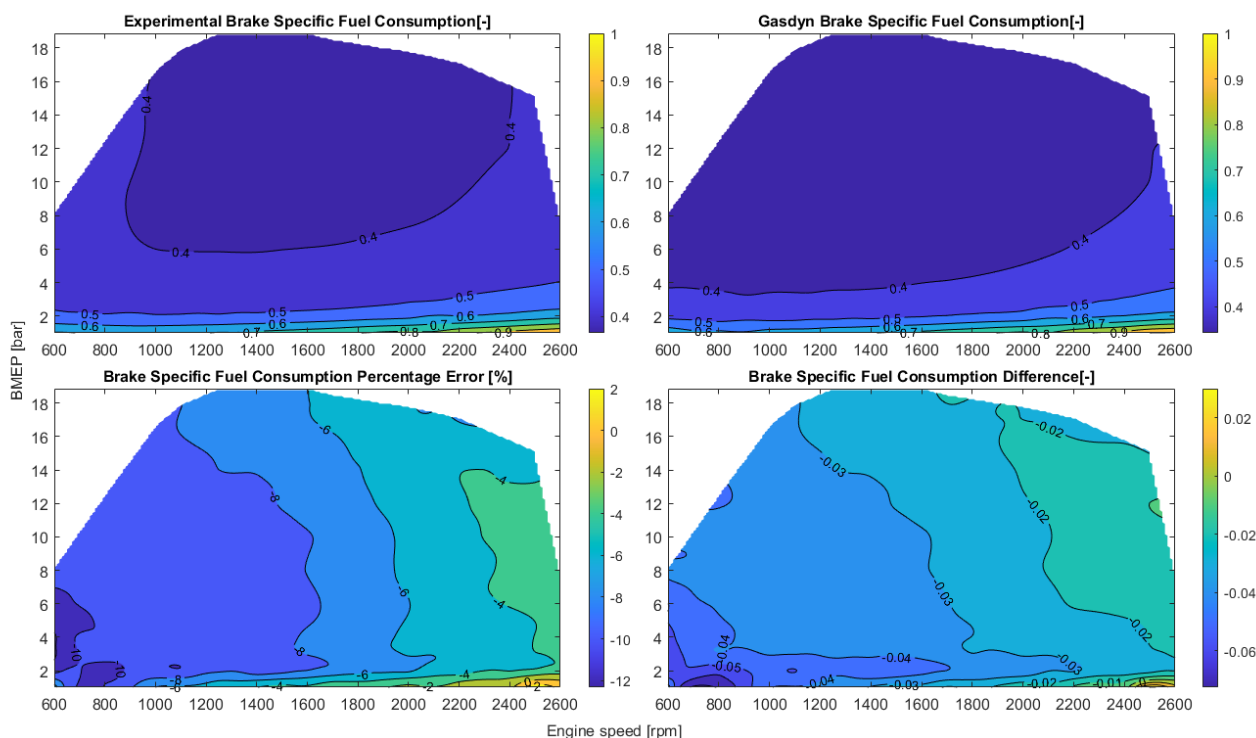


**Figure 9.** Contour plots of the measured and computed Brake Specific Fuel Consumption (BSFC in g/kWh), relative and absolute errors in the whole steady state engine map.

#### Transient Validation

In this paragraph the validation performed under transient conditions is presented. The same 1D engine model is run, varying the engine speed and brake torque required, to simulate the engine behavior during a WHTC driving cycle. The engine speed is imposed, while the engine torque requested to the engine corresponds to the measured torque during the driving cycle. The 1D model exploits an internal PID controller to achieve the requested engine torque, as time proceeds. The resulting engine speed profile is reported in Appendix B, Figure A8. Figure 10 shows the torque profile comparison: the 1D model responds correctly to the changes of torque requested during the WHTC cycle. A comparison of cumulative fuel consumption along the transient is presented in Figure A9,

and the results are satisfactory, showing a final error below 5%. This allows for the use of the 1D model in the complete vehicle simulation platform.

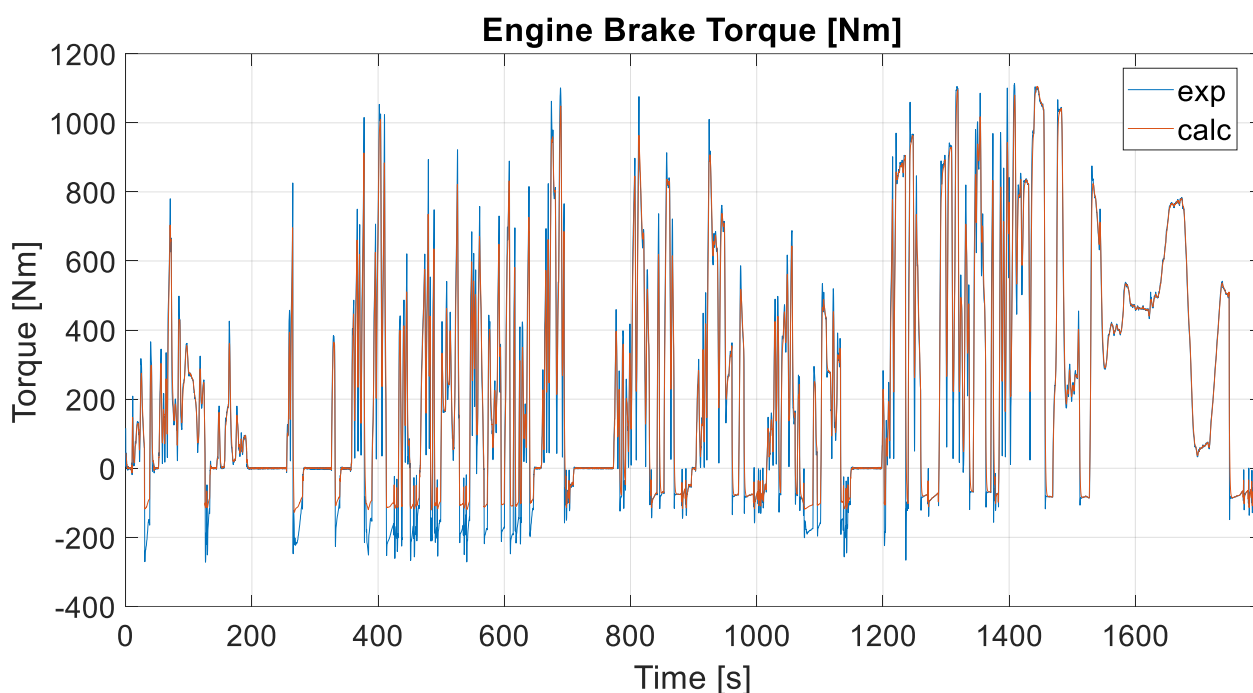


**Figure 10.** Engine brake torque comparison with experimental data during a WHTC driving cycle.

#### 4. Co-Simulation Platform

This section describes the general co-simulation methodology developed to perform a simulation where multiple sub-models are run simultaneously, exchanging input and output signals. To integrate a 1D engine model, as well as the other subsystem models, into the full vehicle system framework, an accurate and flexible tool was required. MATLAB-Simulink was chosen as the main backbone of the simulation platform, due to its widespread use within the industry and its support of many co-simulation protocols, such as S-Functions and FMI/FMUs. All the sub-models making up the vehicle system have been developed and compiled in their own native environment and then converted into a compatible format (S-functions or FMUs) to be integrated into the Simulink environment, as shown in the schematic of Figure 11. This co-simulation framework also allows the rapid exchange or replacement of system components, to vary the vehicle configuration and investigate the effects on the whole coupled system. The partners developed the following sub-models in the EU project Vision-xEV:

- FPT Motorenforschung provided the driveline, mission and vehicle modelling and characterization.
- Politecnico di Milano contributed with the 1D refined and fast simulation model of the IC engine, together with its steady state validation.
- Aristotle University of Thessaloniki (AUTH) modelled the after-treatment system.
- AVL provided the map-based IC engine and HVAC cooling system models.
- University of Ljubljana proposed their electric motor model.
- Vrije Universiteit Brussel (VUB) achieved the battery model.
- Universitat Politècnica de Valencia (UPV) defined the energy management module.

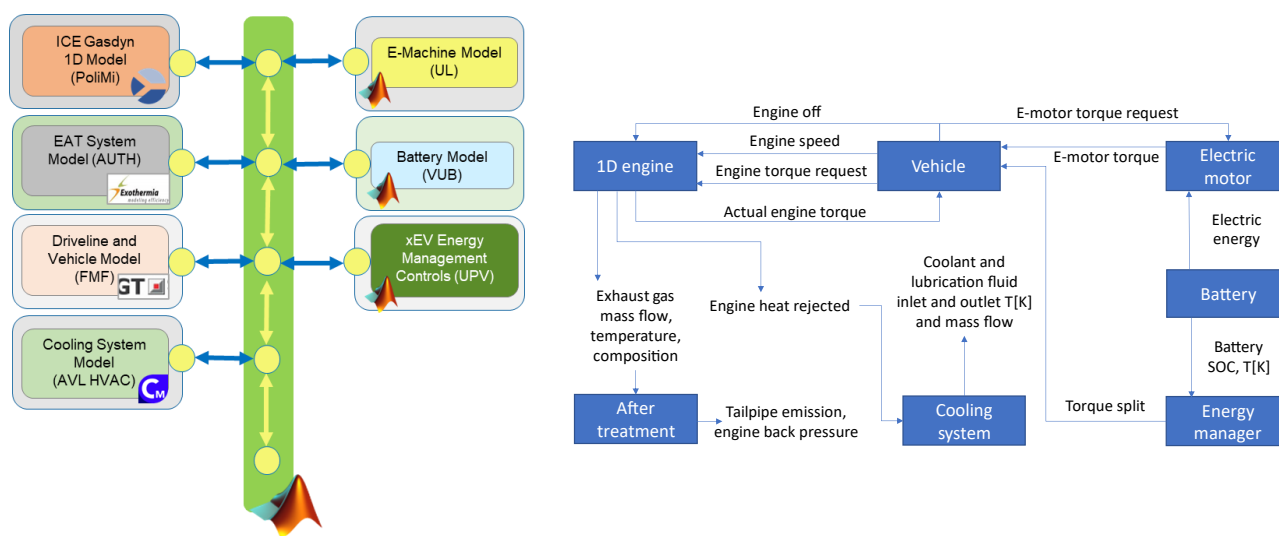


**Figure 11.** Scheme of the co-simulation framework and main signals exchanged.

For clarity, Figure 11 summarizes the main signals exchanged among the sub-models.

The co-simulation consists in a modeling platform where the connected models are all run together. Every model has its own time advancing requirements and suitable time for signal exchange. The hosting platform (Simulink) oversees the entire model, signaling to each module when to proceed with the calculation or wait for signal input/output. This is possible by means of a common communication protocol used in each sub-model, the FMU standard [32].

## 5. Vehicle, Driver and Transmission Model

As a first step towards the coupled vehicle system model, the authors developed the sub-model, which includes the vehicle and the transmission. The model is built with Gamma Technologies (GT) Suite [33], one of the leading CAE software for performance simulation, using specific data available for this application. These data include characteristics about gearbox, torque converter, transmission control strategy, axels configuration, wheels and brake specifications and vehicle mass and drag performances. For validation purposes, the vehicle and transmission models have been coupled to a map-based IC engine model, which uses as inputs the measured engine performance and fuel consumption maps. This approach, albeit simplified, provides a way to run very quick simulations, which were useful to tune the transmission behavior and match the measured data. The model also includes a “driver” PID controller which actuates the accelerator and brake pedal requests, to ensure that the vehicle follows the mission profile.

The model behavior has been validated using two different measurements: the first was a full acceleration test, which helped calibrate not only the upshift behavior, but also the inertias of the transmission and a start-stop cycle. As can be seen in Figures 12 and 13, the model has a very good match with the experimental data, closely replicating the behavior of the vehicle’s transmission.

Once this initial validation work was completed, the map-based engine model was replaced by a link to the Simulink environment, to realize the mechanical coupling between the driveline and the 1D thermo-fluid dynamic engine model and send the driver torque request to the engine. The coupling was achieved as follows: the driver sends a torque request to the engine model in Simulink, which tries to actuate it through a PID controller that varies the injected fuel quantity. The actual torque value given as an output is actuated in GT-ISE, a commercial simulation platform for powertrains and vehicle [33], directly on the transmission input shaft, which delivers as feedback the speed of the engine model. In this way the system was not over-constrained.

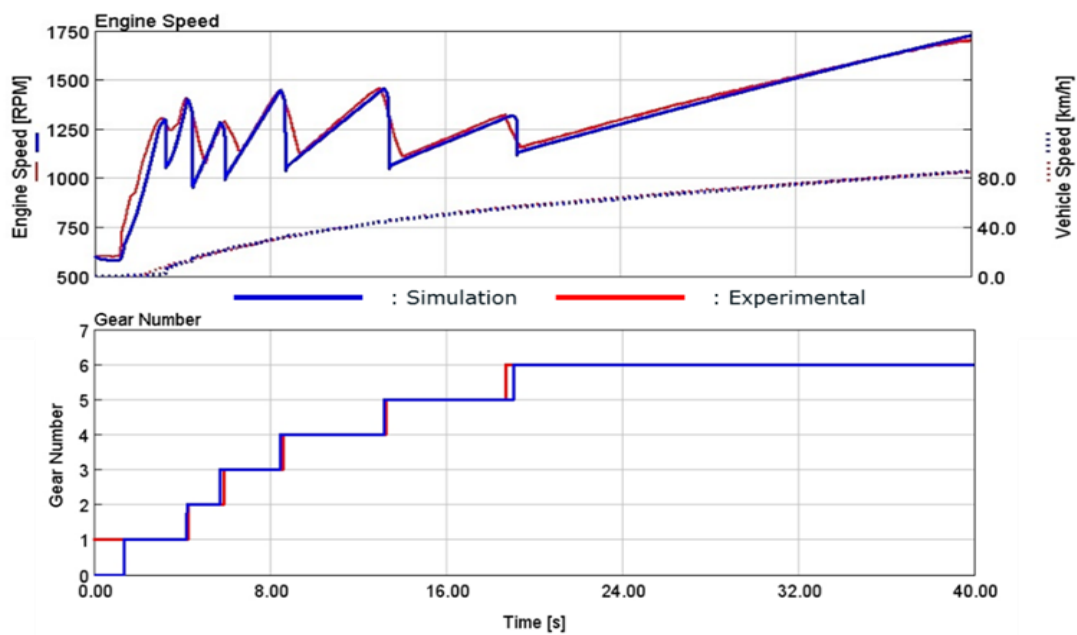


Figure 12. Transmission behavior under full acceleration and comparison with measured data.

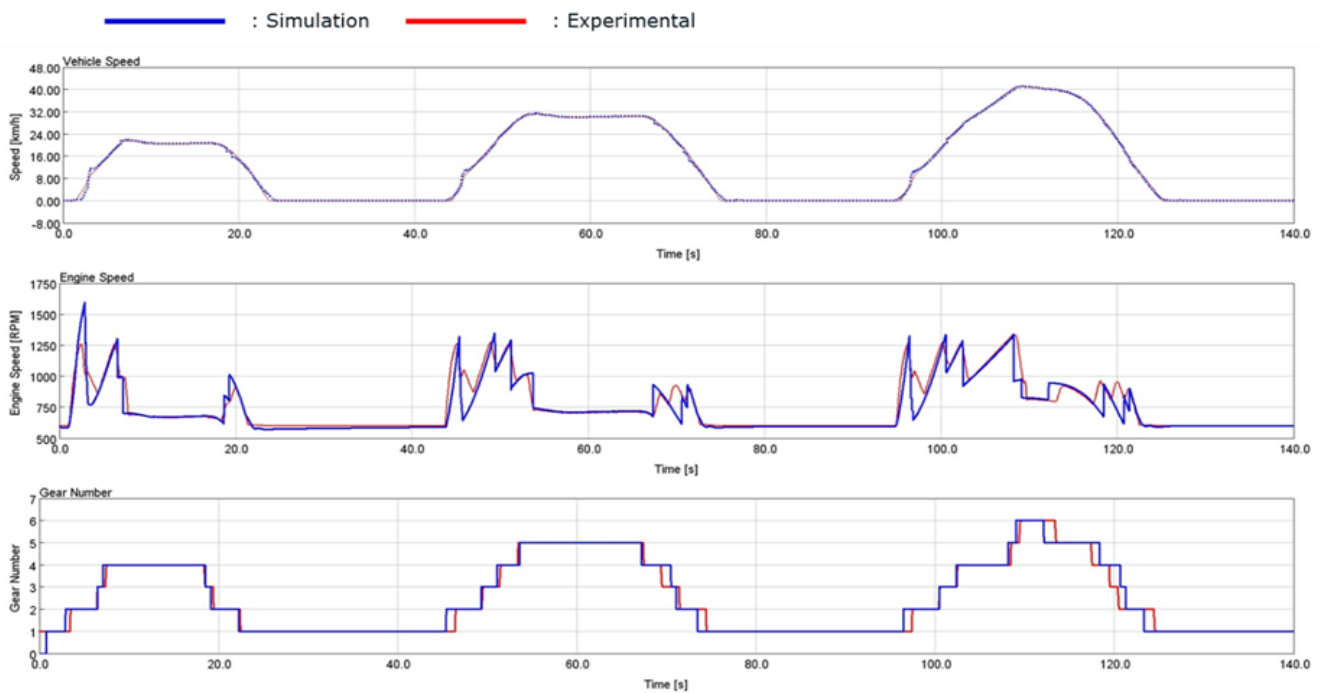


Figure 13. Validation of transmission behavior in start-stop cycle.

## 6. Baseline Model

The first task was to use the co-simulation platform to create a reference baseline case, to which all the other hybrid configuration results could be compared. This configuration, presented in Figure 14, is a digital twin of the non-hybrid HD urban bus, and therefore it includes the following models only:

- vehicle, driver and transmission model (FPT Motorenforschung AG)
- 1D engine model (Politecnico di Milano)
- EU 6 exhaust after-treatment model (Aristotle University of Thessaloniki)
- cooling system model (AVL HVAC).

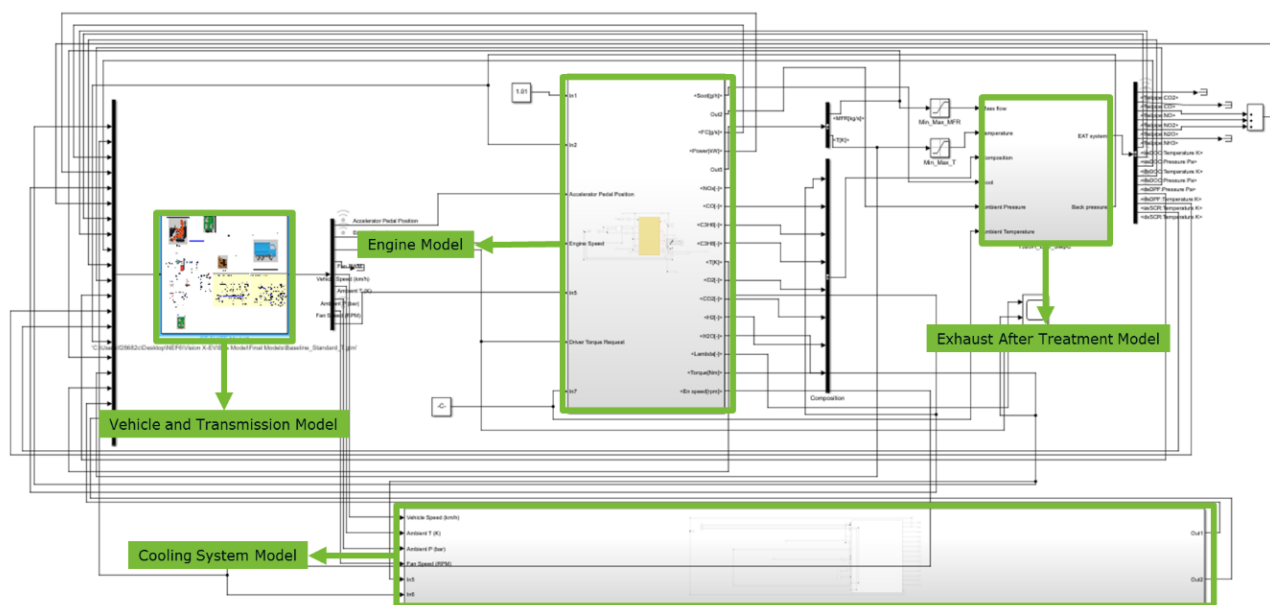


Figure 14. Overview of the baseline co-simulation framework.

The models have been interconnected to exchange data: the vehicle and driveline model sends the torque request to the 1D engine model and sets the engine speed, while it receives the coolant temperature signal from the cooling model, which it uses to define the fan speed, which is then sent back to the cooling model. The 1D engine model has as an output the engine-out exhaust gas flow rate, temperature and composition, which are transferred to the ATS model, which, in return, sets the engine exhaust back-pressure.

### 7. Conventional Architecture Results

The simulation has been run on the whole RDE cycle, which has a duration of 7980 s, with a simulation time to real time ratio around 3:1. The simulation has been repeated for three different ambient conditions: 0 °C, 25 °C and 40 °C, all at the same ambient pressure. This gave the opportunity to check how the ambient temperature affects the fuel consumption and the cooling system, something that is not usually possible to achieve when using a map-based simulation approach. The results are summarized in Table 2. The fuel consumption results confirm that the IC engine model correctly predicts an increase in fuel consumption as the ambient temperature rises. Due to the air-to-air charge cooler used on this engine, the average charge air temperature in the intake manifold increases by about the same amount as the ambient temperature. This has a detrimental effect on volumetric efficiency, reducing the amount of air trapped inside the cylinder during each cycle by over 10% when comparing the same engine speed and load point at 0 °C and 40 °C. The air excess lambda will then be lower, and the combustion efficiency worsens, leading to higher BSFC.

Table 2. Fuel and energy consumption results for baseline architecture (non-hybrid) at different ambient temperatures.

Ambient Temperature [°C]	0	25	40
Total fuel consumption [kg]	11.19	11.45	12.03
Fuel consumption [L/100 km]	34.40	35.22	37.08
Engine positive energy [kWh]	47.5	47.5	47.6
Engine motoring energy [kWh]	−1.7	−1.7	−1.7
Fan energy consumption [kWh]	0.14	0.06	0.05

A difference can be noticed in the NO<sub>x</sub> emissions as well, as reported in Figure 15: at 40 °C the higher temperatures and increased fuel consumption produces an increase of more than 15 g in the cumulated NO<sub>x</sub> engine out emissions, compared with the 25 °C ambient temperature case. For the 0 °C case the results are not reported; however, the authors suggest expecting a reduced amount, in agreement with the trend of Figure 15. This is due to the lower fuel quantity consumed and the cooler in-cylinder fresh charge temperatures.

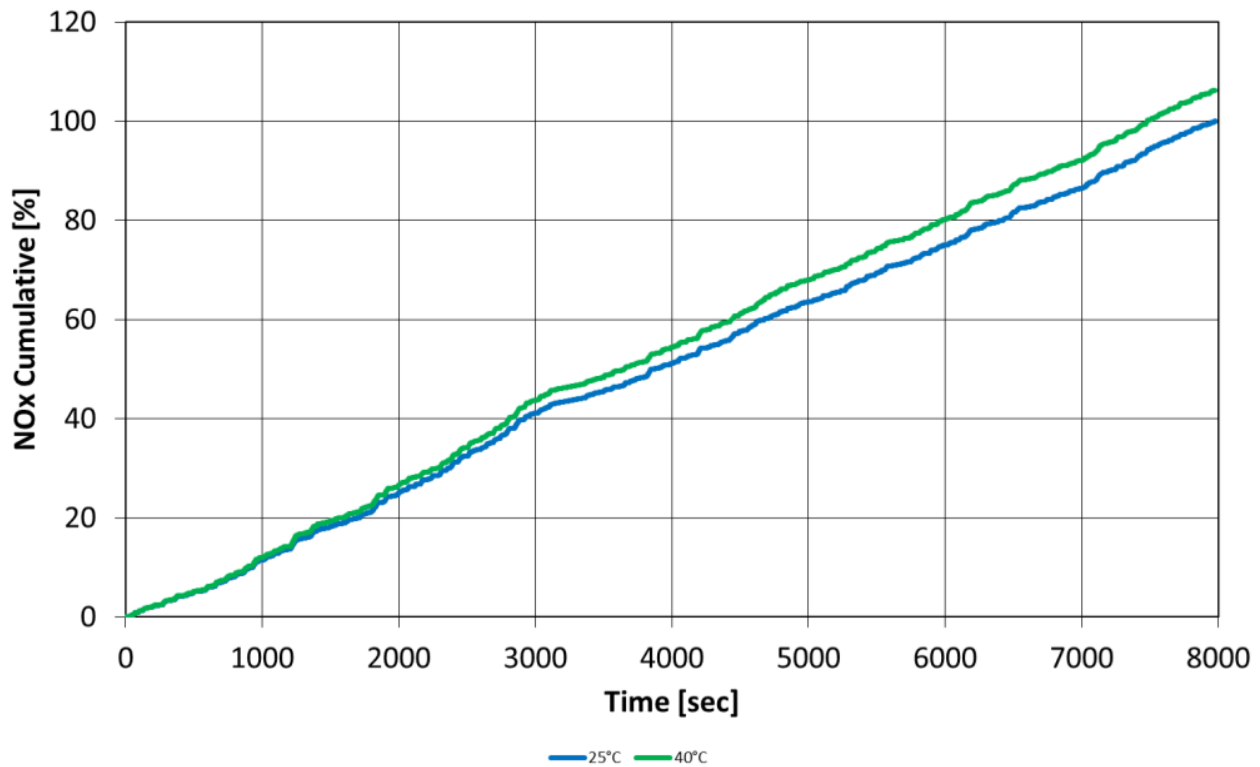


**Figure 15.** Cumulated engine-out NO<sub>x</sub> emissions at 25 °C and 40 °C.

Another consideration regarding the potential of this co-simulation approach is certainly represented by the different response of a complete fluid dynamic-based engine model, compared with the map-based modelling approach. Having a crank angle-resolved fluid dynamic engine model allows for considering the actual engine response and torque build-up, while a map-based approach can only take into account the mechanical inertia of the driveline in the simulation, which helps defining the speed at which the engine gains or loses RPMs but neglects the effect of fluid-dynamic inertia.

In Figure 16 the results of a map-based approach are compared with those obtained using the complete engine model. The first chart shows torque gradients that the real engine would never be able to match, while the results with the complete engine model have much smoother torque pick-ups and drops, especially when transitioning towards negative torque values.

This is particularly important during the development phase in which the engine only, not the vehicle, is to be tested on the bench and the simulations are requested to provide a time-based torque profile, corresponding to a specific vehicle driving a mission. Using the profile calculated by a map-based engine model frequently results in unrealistic transient performance expectations that the test engine is not able to follow.

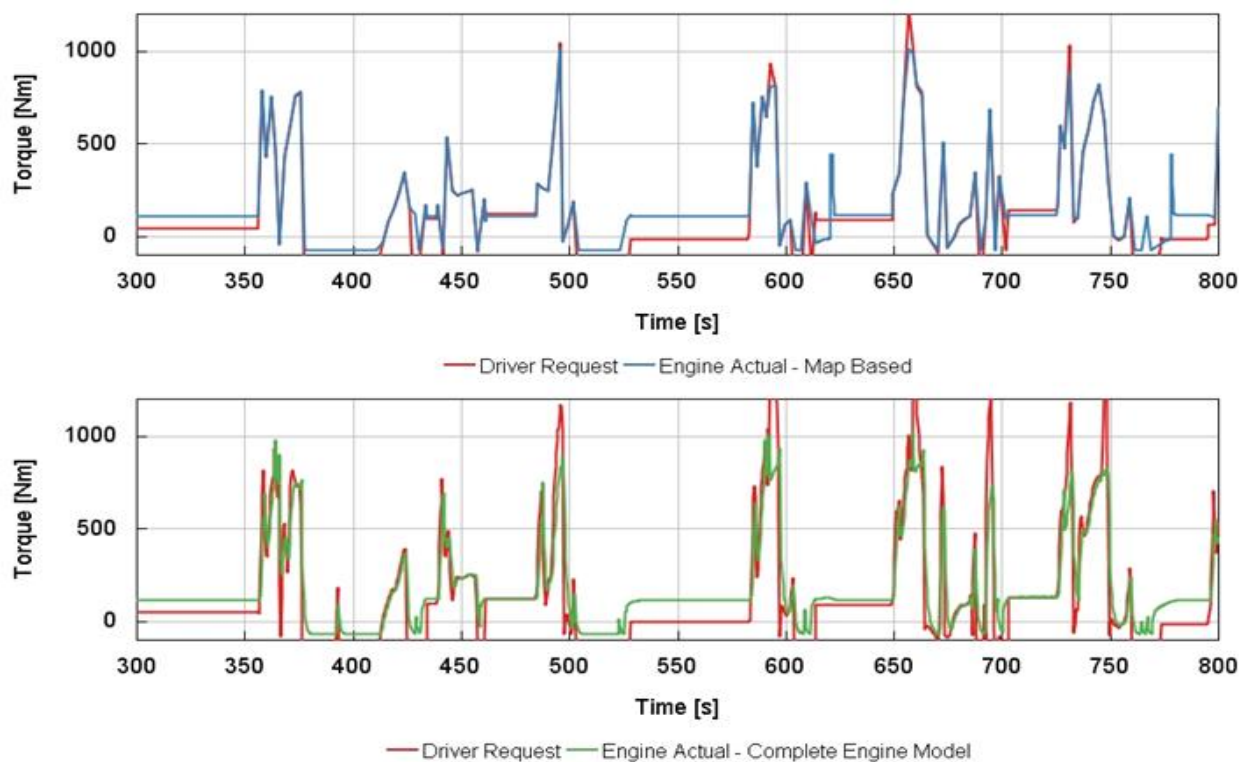


Figure 16. Comparison of torque traces from a map-based and a complete engine model.

### 8. Hybrid Model Performance: Ambient Temperature Effect

In this section the capabilities of the integrated simulation approach are demonstrated in the analysis of a 48 V P1 hybrid system at different ambient temperatures.

As mentioned in previous sections, an urban bus is a perfect candidate to exploit the benefits of low-voltage hybridization: the frequent start-stops and the low vehicle top speed achieved during the mission determine a constant supply of kinetical energy that can be recovered with a relatively low power electric machine, thus avoiding the cost and complications of resorting to a high-voltage application, which would have a negative impact on the overall cost of ownership of the vehicle.

During the usual development process, it is difficult to have access to the information necessary to characterize the thermal behavior of the electric components: normally in the first stages of a project, the electric machine and battery are modelled using simple performance and internal losses maps, which has an impact on the reliability of the simulation results. However, thanks to the integrated simulation approach, it was possible to integrate in the co-simulation the high-fidelity models of the electric machine and battery developed by the European project partners, which allow for more detailed performance results.

In parallel to the simulation framework setup, the requirements of the P1 hybrid components have been defined. The electric machine characteristics have been selected using data gathered during the simulation of similar applications and are reported in Figure 17. The battery cells configuration has been chosen starting from the cell characteristics by considering the system voltage and the capacity needed to feed a relatively powerful e-machine, such as the one that has been chosen in this case.

Together with the hardware components also the control strategy was elaborated. The control strategy is responsible of finding the best torque split value between the internal combustion engine and the electric machine, while respecting the constraints on the maximum temperature of the air-cooled battery, which should not exceed 45 °C, and excluding any kind of boosting and start-stop function when the engine was still heating up, to avoid prolonging the ATS warm-up phase and raising the tailpipe emissions. This is another benefit of the integrated simulation framework approach, since having the inputs

from all the vehicle sub-systems helps refine the control strategy of the hybrid system in ways that are not possible with the traditional simulation procedures, which prevent over- or under-stating the benefit of hybridization in the real world.

System Nominal Voltage	48 V
EM Peak Power	26 kW
EM Continuous Power	16 kW
EM Peak Torque	205 Nm
EM Continuous Torque	120 Nm
Battery Cells Configuration	21 s2p
Battery Capacity	46 Ah
Battery Energy	2.2 kWh

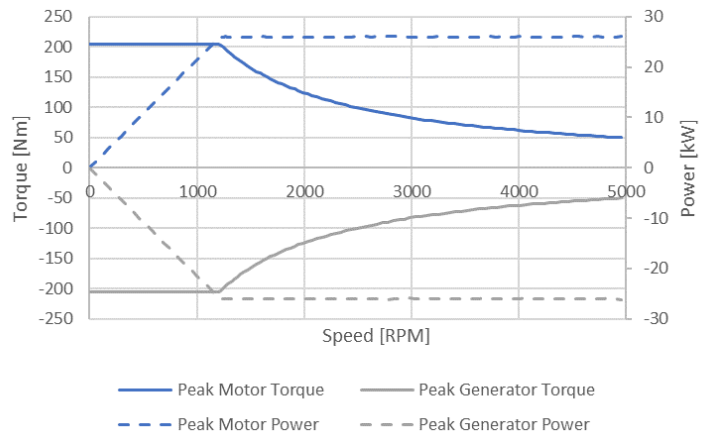


Figure 17. P1 hybrid components specifications and electric machine peak performance curves.

The cooling system has also been updated to include a separate low temperature circuit to serve the electric machine. The radiator has been put in front of the one for the high-temperature cooling circuit, thus cooled using the same fan, while the pump is driven by a viscous clutch and its operational speed is controlled by a simple temperature-based logic.

For this study, the bus vehicle model has been modified to describe the hybrid bus. In particular the following models have been added to the co-simulation framework to achieve a complete model of a hybrid bus.

These additional models have been developed by the partners during the EU project Vision-xEV activities.

- Battery model developed by the University Vrije Universiteit Brussel
- Electric machine model by the University of Ljubljana
- Energy manager model provided by the Universitat Politècnica de Valencia

Figure 18 presents the coupled simulation environment with each sub-model connected to the required models.

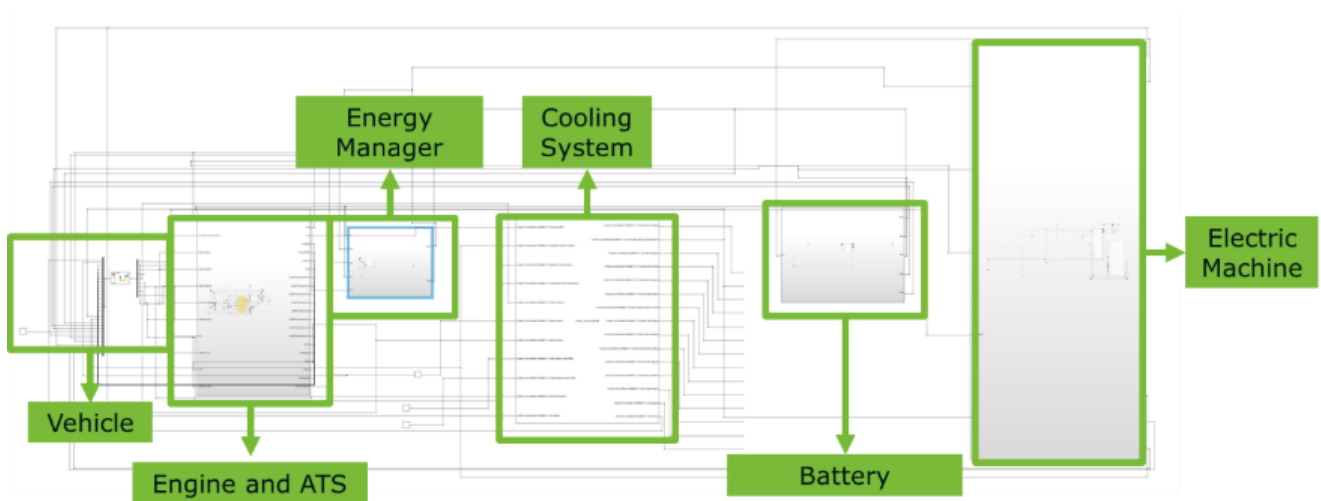
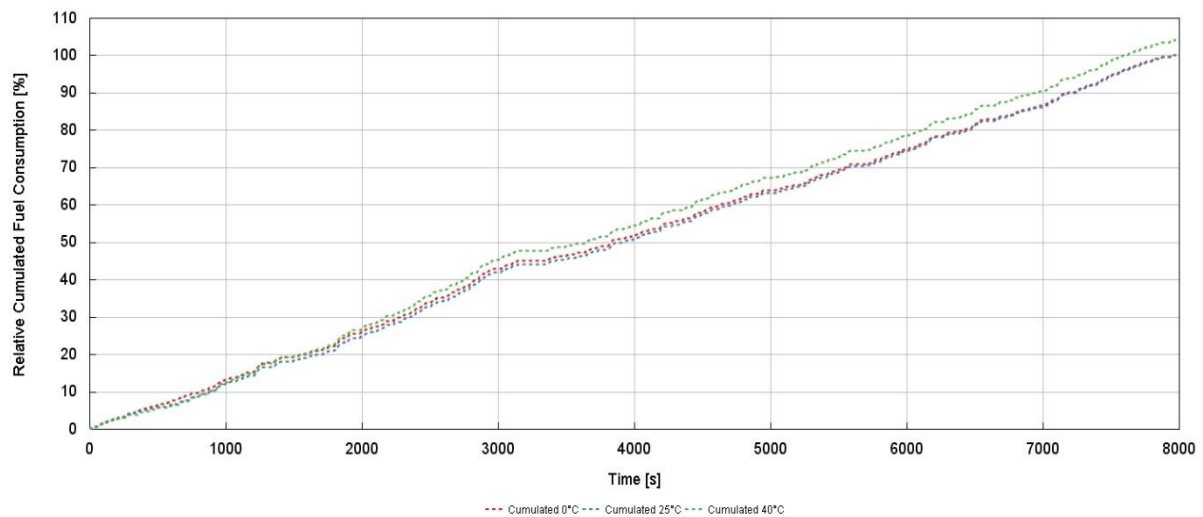


Figure 18. Overview of the co-simulation framework.

As with the baseline case, the chosen ambient conditions were 0 °C, 25 °C and 40 °C. The initial state of charge of the battery for all cases was chosen to be 50%.

The main goal was to assess the impact on the whole vehicle system of different behavior of the sub-systems under very high or very low temperatures.

The engine fuel consumption chart displayed in Figure 19 shows that the improvement in fuel consumption compared to the baseline cases is around 15% and confirms the fact that this mix of vehicle and mission is a perfect match for low voltage hybridization.



**Figure 19.** Fuel consumption comparison for P1 in different ambient conditions.

Analyzing the distribution of the operating points of the electric machine on its performance chart in Figure 20, it is readily apparent that for this application the electric machine is slightly oversized. The electric machine works almost always at part load and is used within a limited range of speed, which suggests that using a smaller electric machine would yield very similar results.

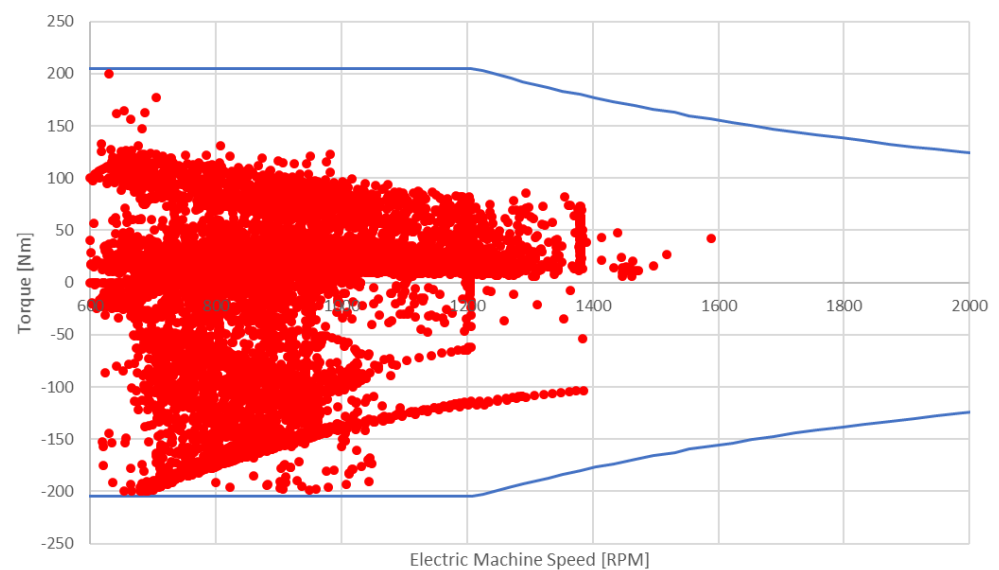


**Figure 20.** Electric machine operating points (red dots) during the driving cycle simulation. Electric machine possible operating range (blue lines).

Thanks to the integrated simulation approach, a detailed analysis of the efficiency of the electric machine can also be made. The model of the electric machine [34] correctly computes the effects of thermal derating on the efficiency presented in Figure 21, which dips below 50% in the final part of the mission. This kind of data is of paramount importance in determining the actual performance of the hybrid system on the mission, and it greatly improves the quality of the simulation results.

On the battery side, thanks to the model [35], an accurate calculation of the losses in the battery is made, further enhancing the quality of the simulation results.

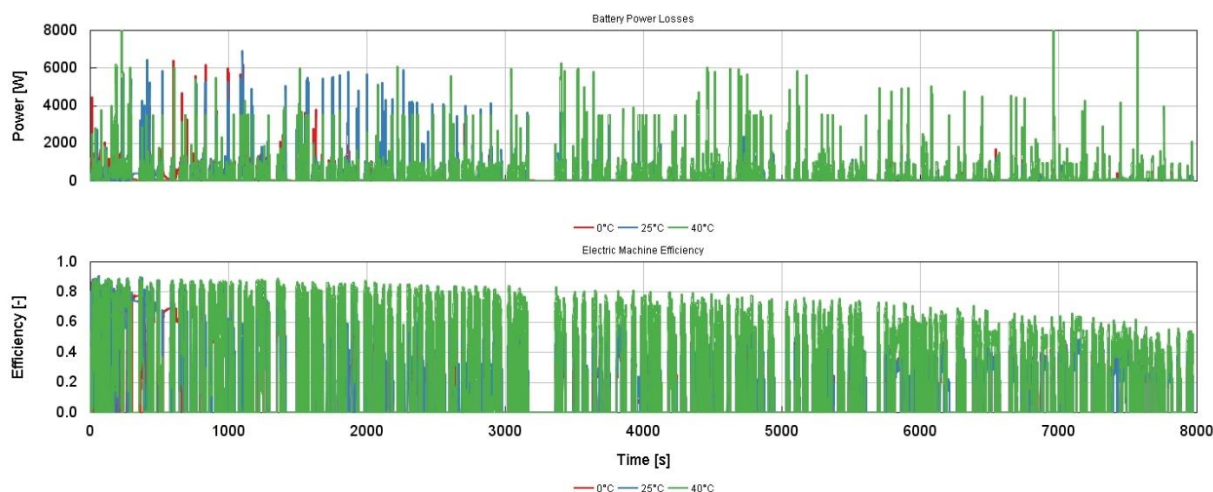


Figure 21. Electric machine efficiency and battery power losses.

Analyzing the IC engine and electric machine power split for the three different cases of Figures 22–24, respectively, what is immediately apparent is that the ambient temperature has a meaningful impact on the duration of the warm-up phase, which stretches from 140 s long at 40 °C up to 600 s at 0 °C. As can be seen by the profile of the engine speed and electric machine torque, during this phase the electric machine is used only for energy recuperation during braking events, and the start-stop functionality is disabled; thus, the engine speed never drops below 650 RPM.

What is also clearly noticeable is the derating in the performance of the electric machine. After the first 2000 s the maximum and minimum torque that it can provide starts decreasing, and by the end of the mission for the 0 °C and 25 °C the maximum positive torque is limited to 15 Nm, while the peak negative torque has diminished to  $-90$  Nm. This imbalance also causes the battery SOC to saturate at 100%, since the motor is not able to spend as much energy as it recuperates during the braking events.

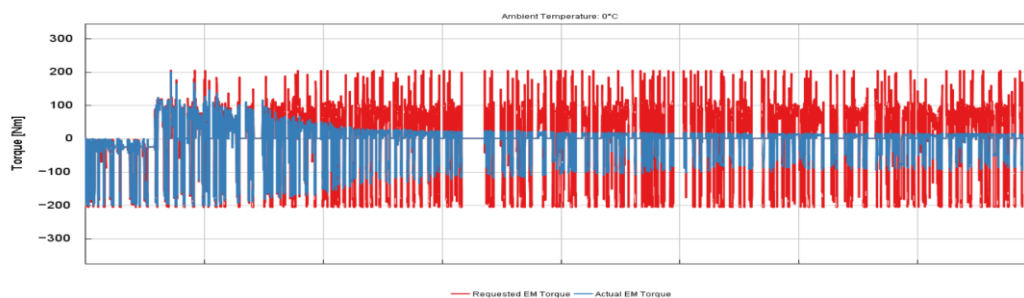


Figure 22. Cont.

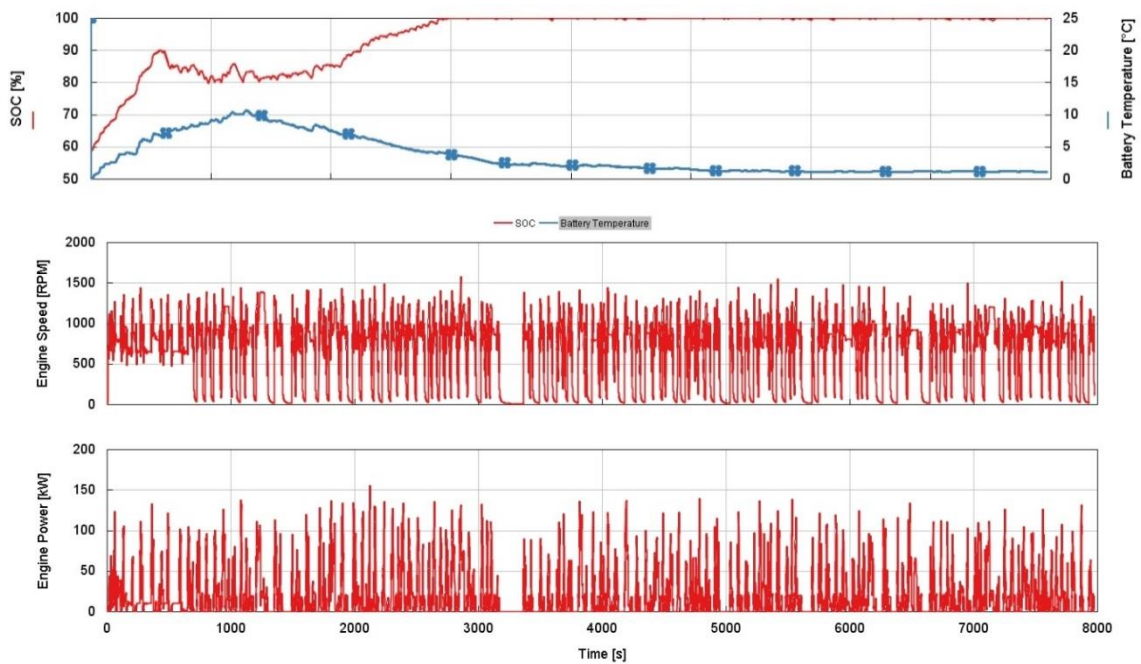


Figure 22. Engine, battery and e-machine performance at 0 °C.

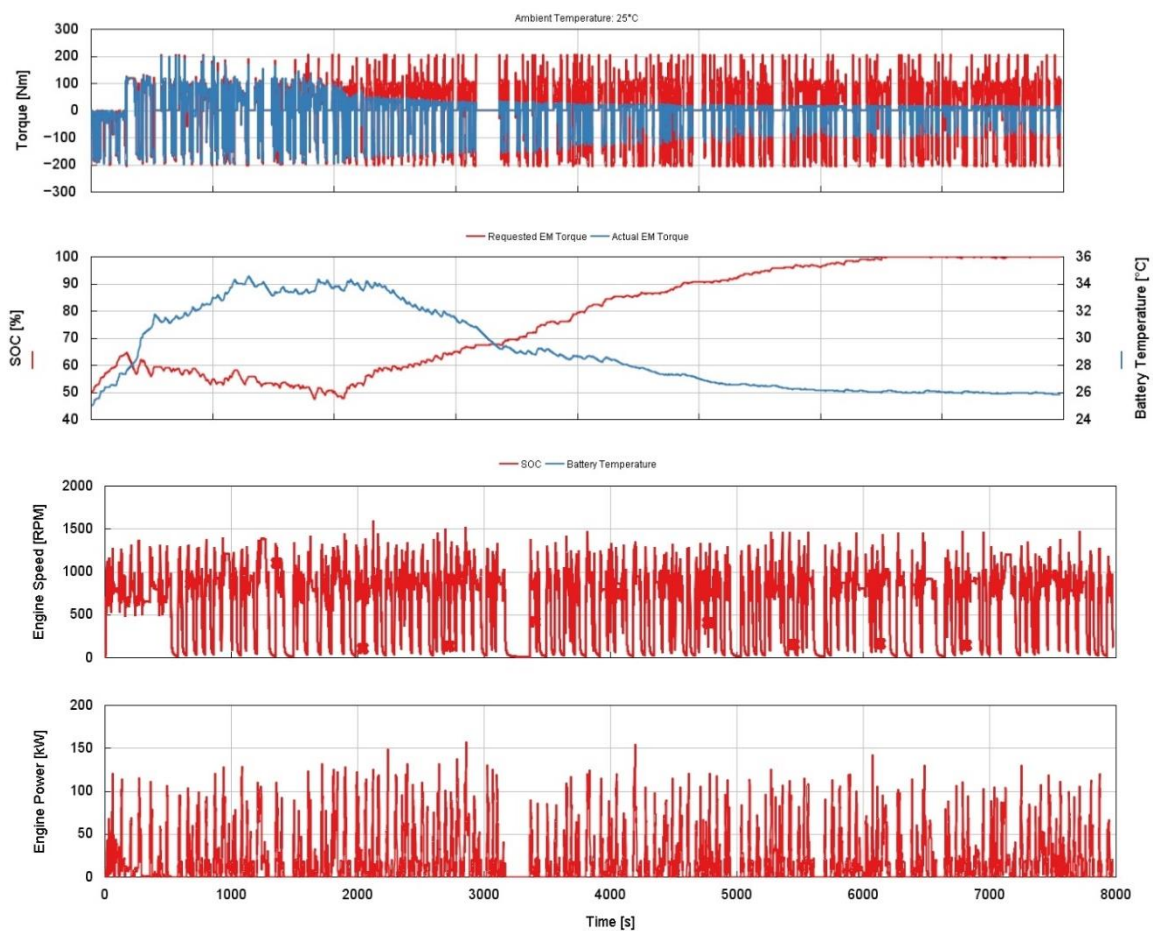
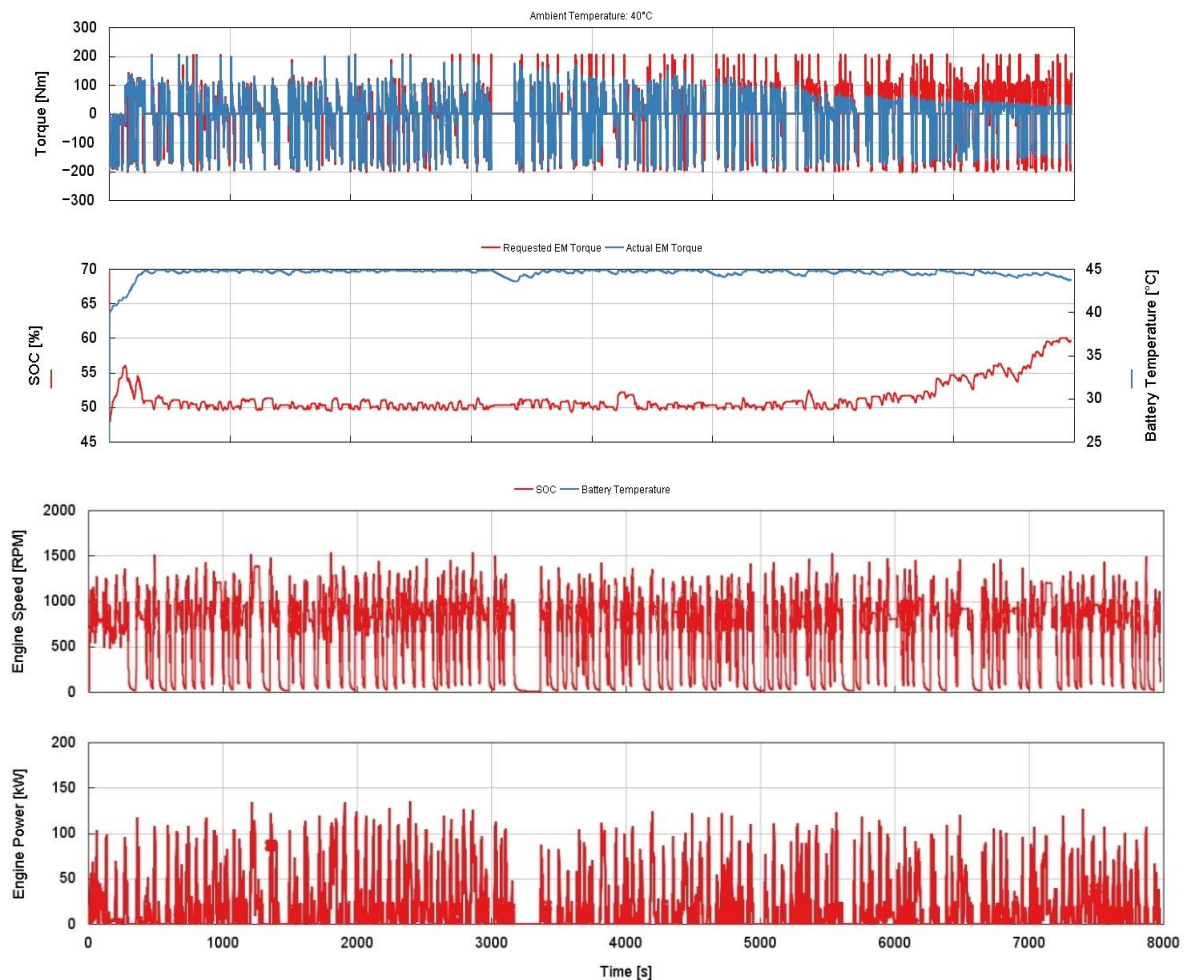


Figure 23. Engine, battery and e-machine performance at 25 °C.

The behavior of the system is different for the case at 40 °C ambient temperature. In this case the use of the electric machine is limited at the energy manager level by the battery temperature, which is not supposed to exceed 45 °C. In the traces below it is noticeable that the energy manager relies much more on the internal combustion engine and friction brakes and requests the intervention of the electric machine less often than in the previous cases, which is why the performance derating starts showing only towards the end of the mission, allowing the final battery SOC to be maintained below 60%.



**Figure 24.** Engine, battery and e-machine performance at 40 °C.

Overall, what is clear from the machine behavior is that the thermal derating plays a major role in defining the performance of the hybrid system, much more than the battery temperature, unless the ambient conditions force it to operate with a very high ambient temperature. Should this be the case for a significant percentage of the vehicle's life, then a water-cooled battery should be investigated.

For what concerns the electric machine cooling, presented in Figure 25, the coolant temperature does not show significant spikes during the mission, and the values are always close to the ambient temperature of each case, which means that the system is well suited for the cooling of the machine. The pump has an almost negligible power draw of 60 W at 0 °C and 25 °C, since the coolant temperature is always low enough that the pump itself stays at the idle speed of 200 RPM most of the mission, but at 40 °C the pump is forced to spin at 600 RPM to keep the coolant temperature in check. This translates into a not negligible 1 kWh of additional energy spent by the pump during the mission, compared to the lower temperature cases.

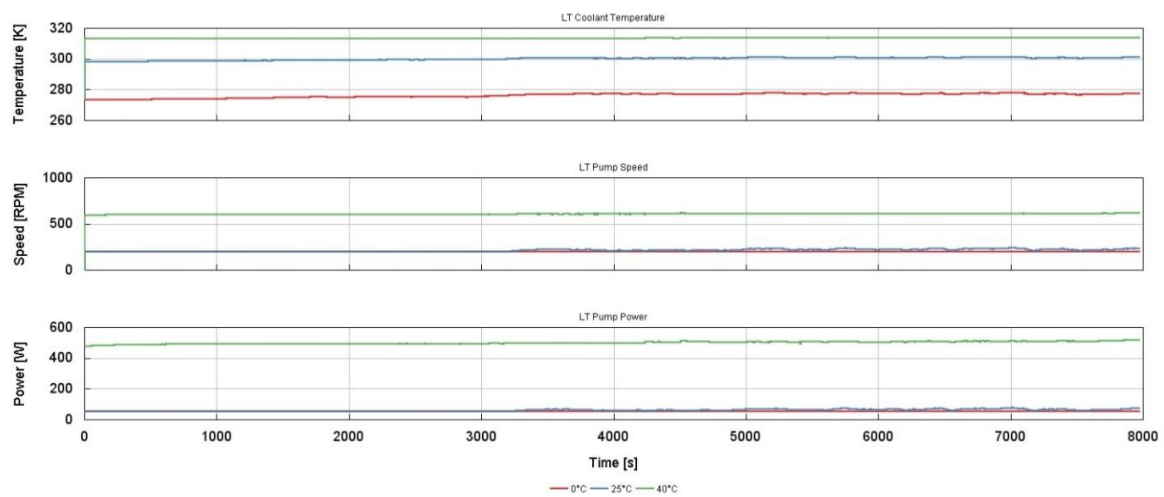


Figure 25. Low temperature (LT) case circuit coolant temperature and pump power.

On the high-temperature cooling circuit shown in Figure 26, there does not seem to have been a significant change in the performance of the radiator and fan following the addition of the low-temperature cooling circuit radiator in front of it. The overall energy consumption of the fan is negative, due to a windmilling effect of the fan cooler blades, predicted by the cooling system model, due to the air flowing through the fan at the given vehicle speed.

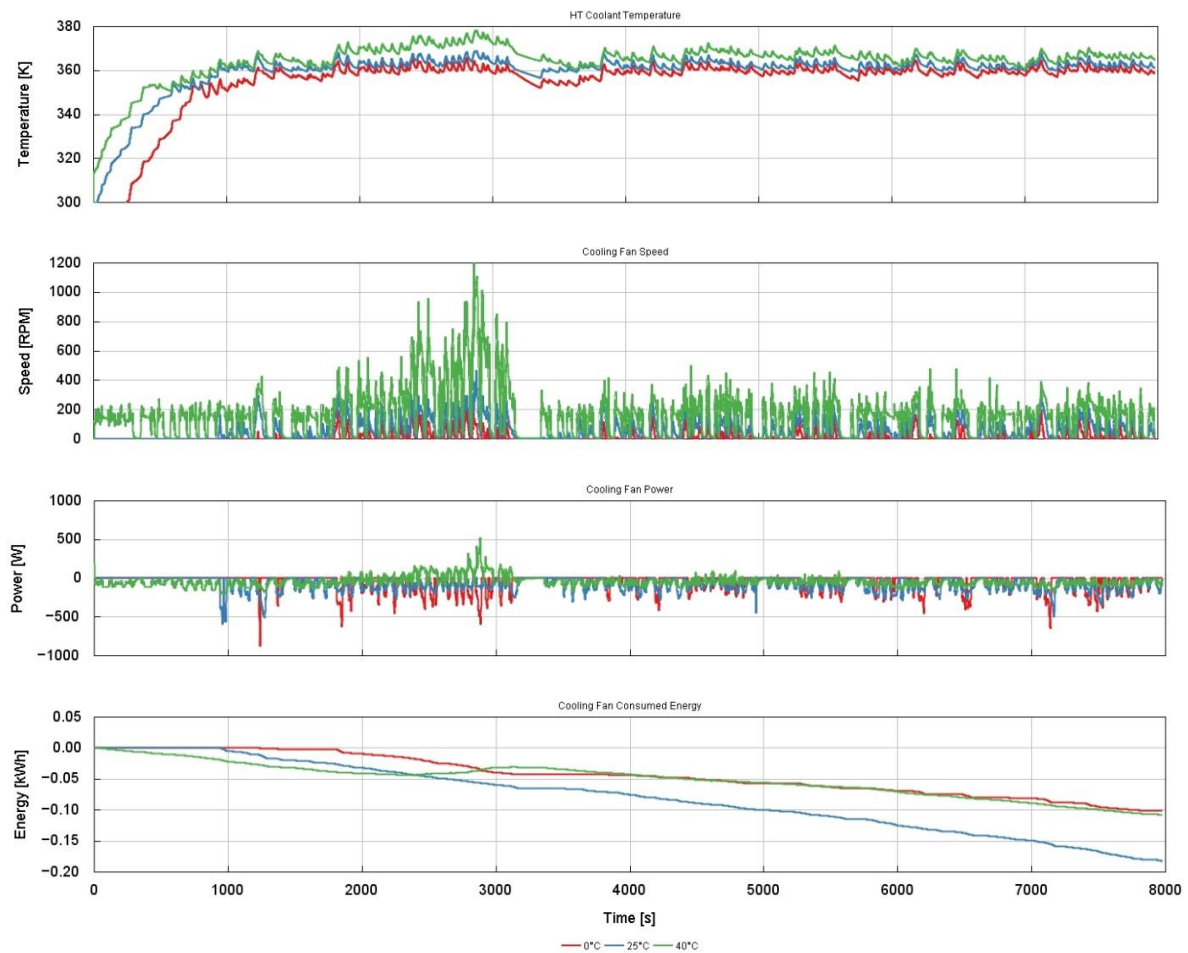


Figure 26. Cooling fan speed, power and consumed energy profiles during mission at different ambient temperatures.

A summary of the vehicle performance is reported in Table 3. It is possible to see that the low ambient temperature helps the cooling of the battery, withdrawing less power for the respective cooling and improving fuel efficiency. Consequently, also the regenerative power of the electric motor reduces with the increase of ambient temperature, since the electric machine is less efficient at higher temperature.

**Table 3.** Fuel and energy consumption results for P1 architecture (hybrid) at different ambient temperatures.

Ambient Temperature [°C]	0	25	40
Total fuel consumption [kg]	9.670	9.672	10.060
Reduction compared to baseline [%]	−13.6	−15.6	−16.4
Fuel consumption [L/100 km]	29.8	29.8	31.0
Engine positive energy [kWh]	41.2	41	41.8
Electric motor boosting energy [kWh]	2.1	2.85	3.24
Electric motor braking energy [kWh]	−4.00	−4.49	−3.89
Battery energy loss [kWh]	0.34	0.39	0.49
Fan energy consumption [kWh]	−0.14	−0.06	−0.05

## 9. Conclusions

This paper has covered the activities related to the implementation of a flexible simulation framework for a 12-m heavy-duty city bus. The tool has been used as a digital twin to demonstrate the potential of the integrated simulation framework and applied it on a real case study. The baseline conventional powertrain has been compared to the hybridized powertrain, highlighting the advantages. Thanks to the co-simulation methodology, it was possible to evaluate the correctness of the sub-component size or dimensioning. These achievements have a deep impact on the simulation accuracy and allow a reduction of development time for electrified vehicles. On the simulation side, the use of a fully transient 1D engine model allows to reproduce the real response and capabilities of the engine. This is crucial to correctly predict the RDE cycle emissions and consumptions, thanks to the intrinsic unsteady nature of the 1D model. Additionally, the computational effort has been reduced to exploit the 1D model solution in reasonable CPU/real time ratio.

The results of the case study also underline the importance of conducting performance analysis using high fidelity system sub-models. This approach allows not only to accurately assess the behavior under different workloads or working conditions, but also the interactions between the modelled sub-systems and their contribution to the vehicle performance. As an example, with a traditional “map based” approach the effect of thermal derating of the electric machine and the battery would have been impossible to quantify, which would have had an impact first on the results of the simulation and potentially on the development cycle of the electrified vehicle.

**Author Contributions:** Conceptualization, A.O. and S.L.; methodology, A.O. and S.L.; software, A.M.M. and G.M.D.V.; validation, A.M.M. and G.M.D.V.; formal analysis, A.M.M.; investigation, A.M.M. and G.M.D.V.; resources, A.M.M.; data curation, G.M.D.V.; writing—original draft and reviewing, A.M.M. and G.M.D.V.; supervision, A.O. and S.L. All authors have read and agreed to the published version of the manuscript.

**Funding:** This research was funded by the European Union, grant number 824314.

**Data Availability Statement:** Confidential data.

**Acknowledgments:** The authors would like to thank the European Union (EU) project Vision-xEV (Virtual Component and System Integration for Efficient Electrified Vehicle Development), under which they received funding from the EU Horizon 2020 research and innovation program, grant agreement n° 824314.

**Conflicts of Interest:** The authors declare no conflict of interest.

### Abbreviations

ATS	Exhaust After-Treatment System
AUTH	Aristotle University Thessaloniki
BMEP	Brake Mean Effective Pressure
BSFC	Brake-Specific Fuel Consumption
CG	Corberán–Gascón
CFL	Courant–Friedrichs–Lewy
CUC	Clean-Up Catalyst
eCAT	Electrically Heated Catalyst
E-Machine	Electric Machine
EU	European Union
FMF	FPT-Motorenforschung
FMI/FMU	Functional Mock-Up Interface
FSM	Fast Simulation Method
GT	Gamma Technologies
HD	Heavy-Duty
HVAC	Heating Ventilation and Air-Conditioning
ICE	Internal Combustion Engine
NM	Normal Mode
PEMS	Portable Emission Measuring System
PID	Proportional Integrative Derivative
RHU	Rapid Heat-Up
SCR	Selective Catalytic Reactor
SOC	State of Charge
SOI	Start of Injection
RPM	Revolutions per Minute
TUB	Technischen Universität Berlin
TVD	Total Variation Diminishing
UL	University of Ljubljana
UPV	Universitat Politècnica de València
VUB	Vrije Universiteit Brussel
VECTO	Vehicle Energy Consumption Calculation TOol
WHTC	World Harmonized Transient Cycle

### Appendix A

This appendix describes the results regarding the steady state validation of the 1D engine model, discussed in Section 3.

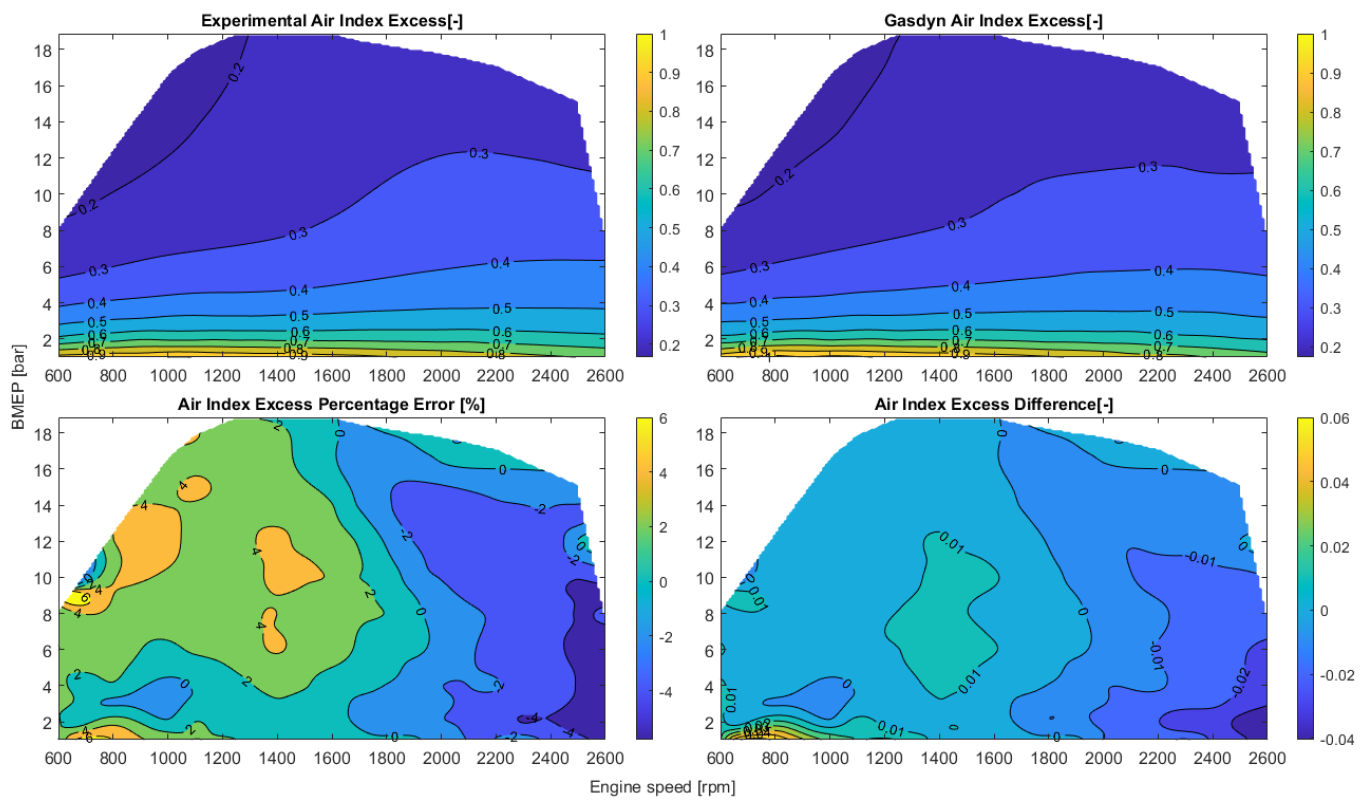


Figure A1. Contour plots of the measured and computed air index excess; relative and absolute errors on the whole steady state engine map.

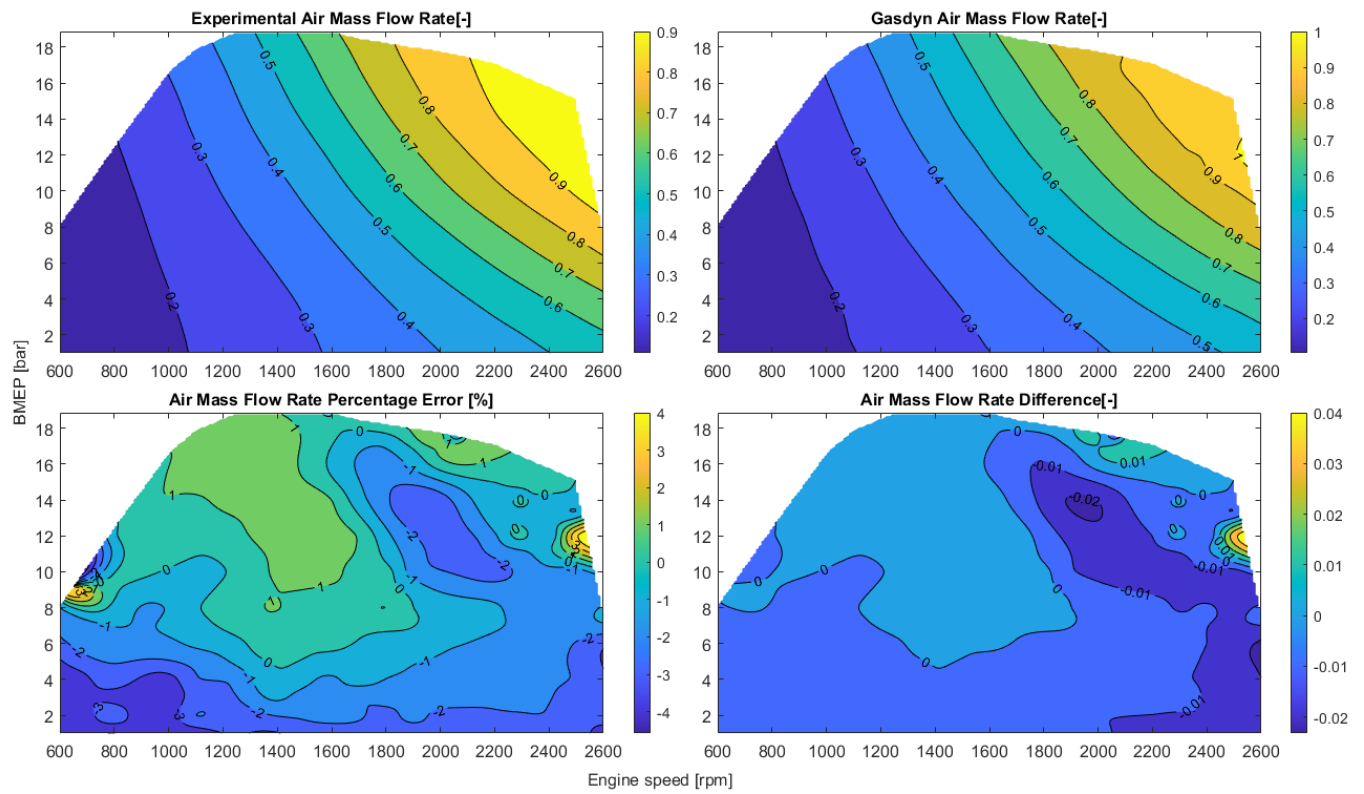


Figure A2. Contour plots of the measured and computed air mass flow rate, relative and absolute errors on the whole steady state engine map.

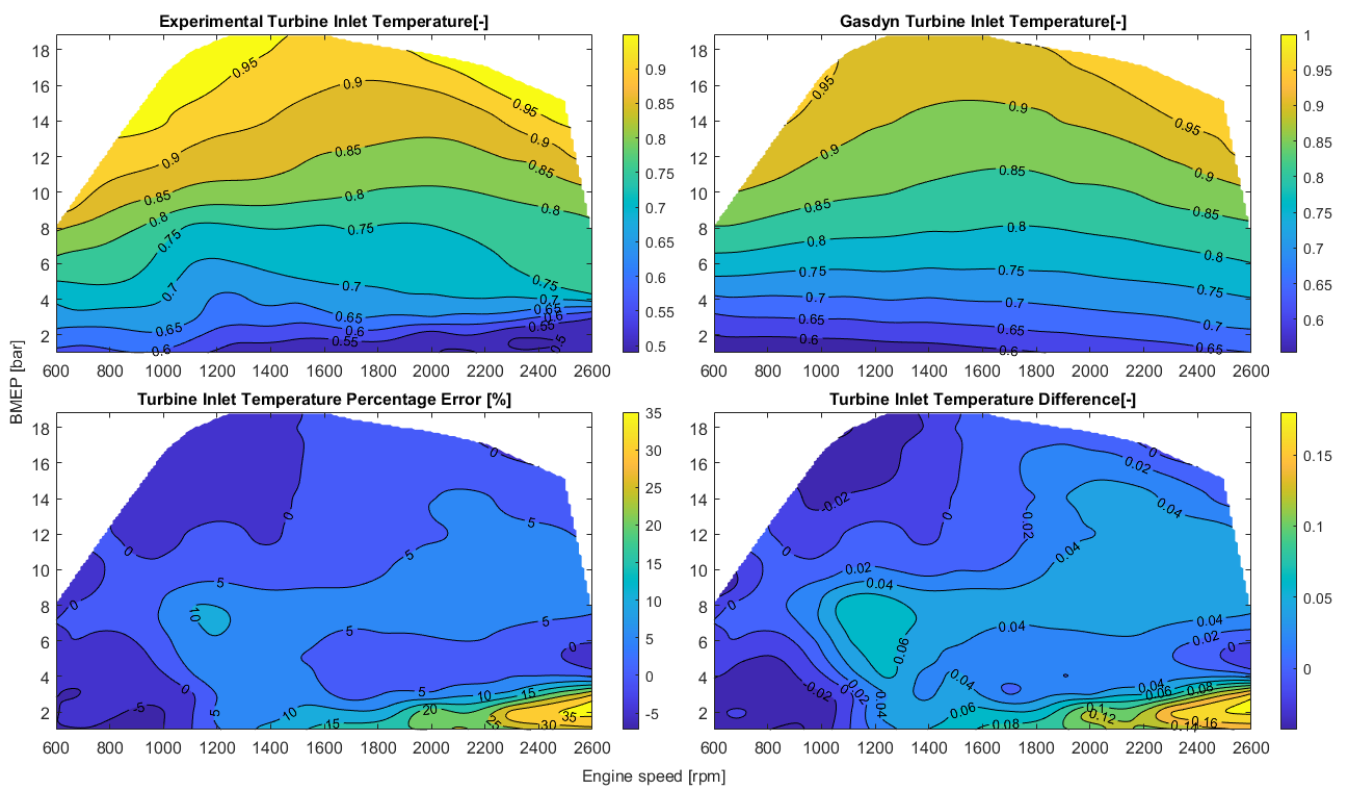


Figure A3. Contour plots of the measured and computed temperature upstream of the turbine relative and absolute errors on the whole steady state engine map.

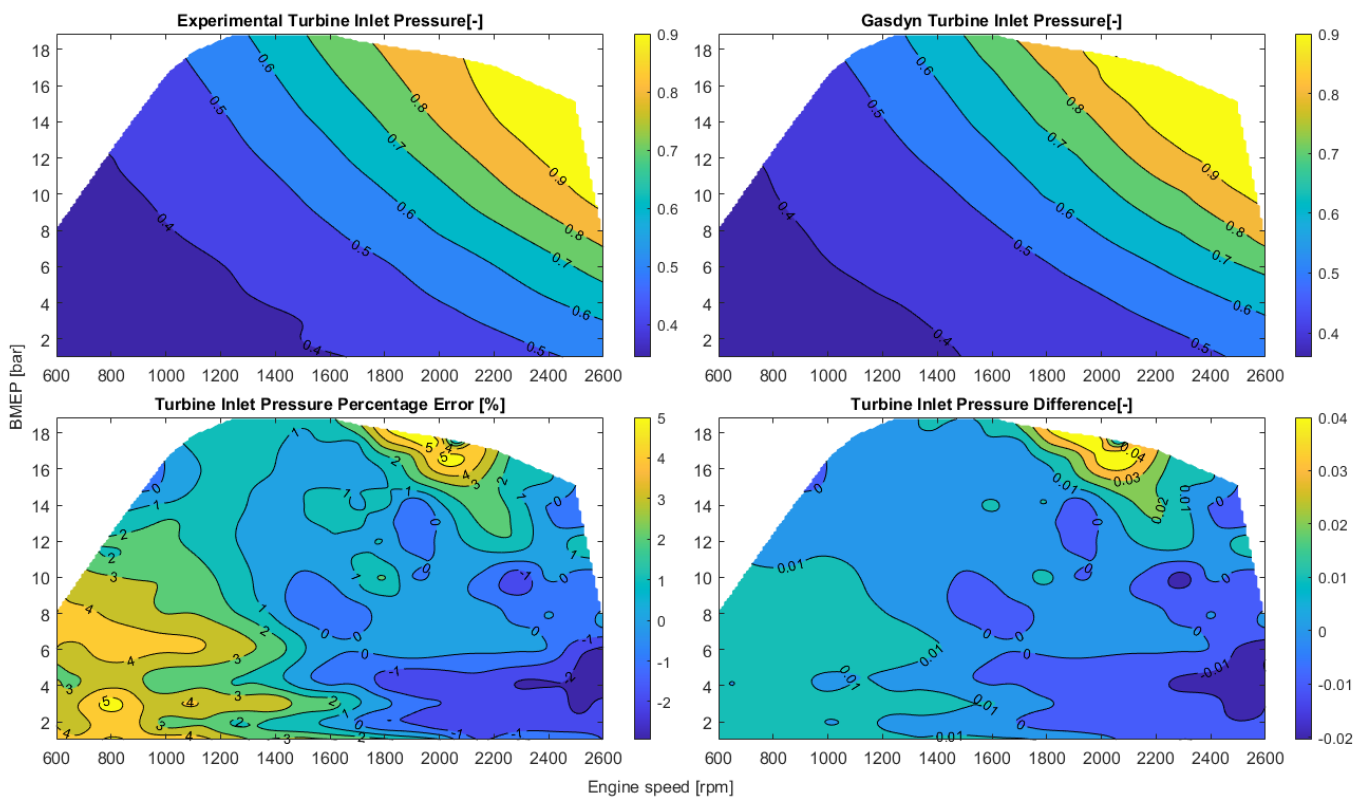


Figure A4. Contour plots of the measured and computed pressure upstream of the turbine relative and absolute errors on the whole steady state engine map.

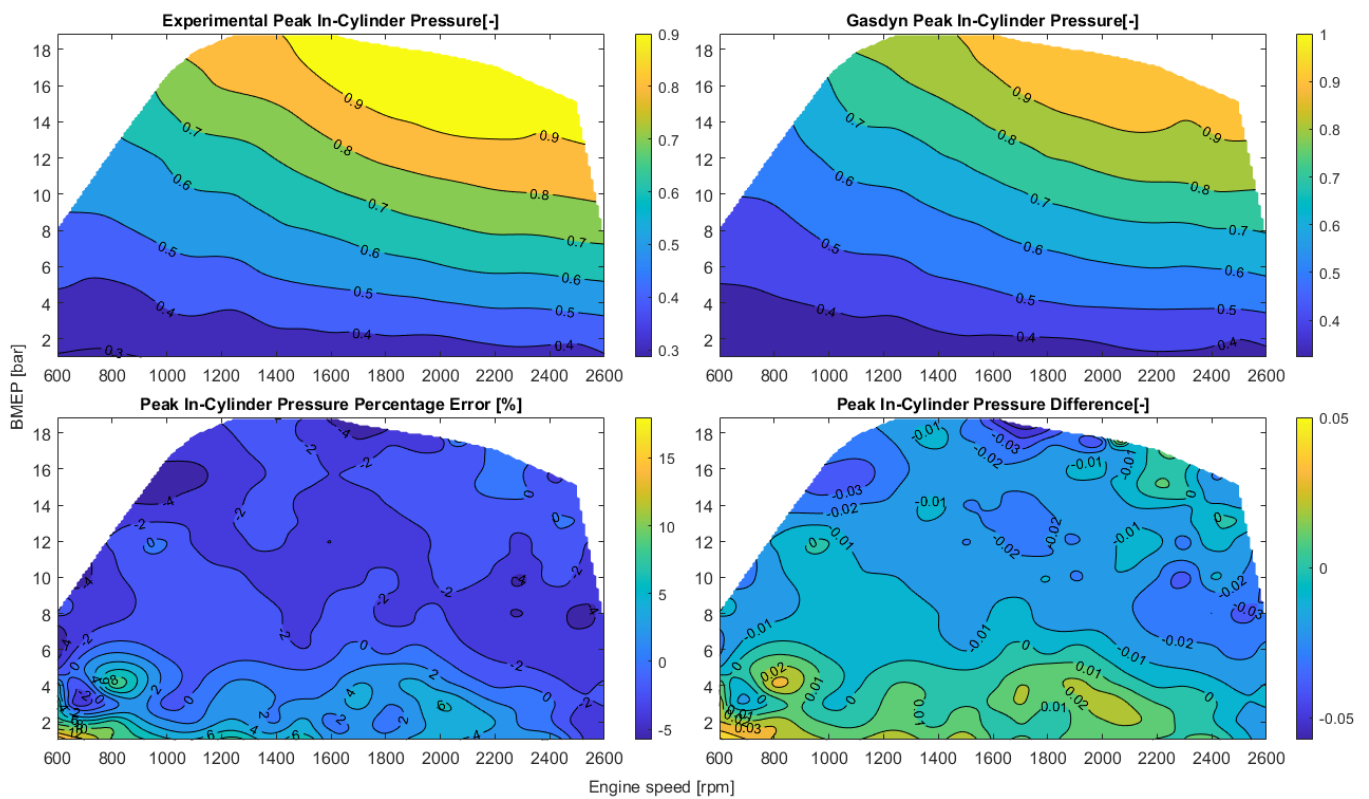


Figure A5. Contour plots of the measured and computed maximum cylinder pressure relative and absolute errors on the whole steady engine map.

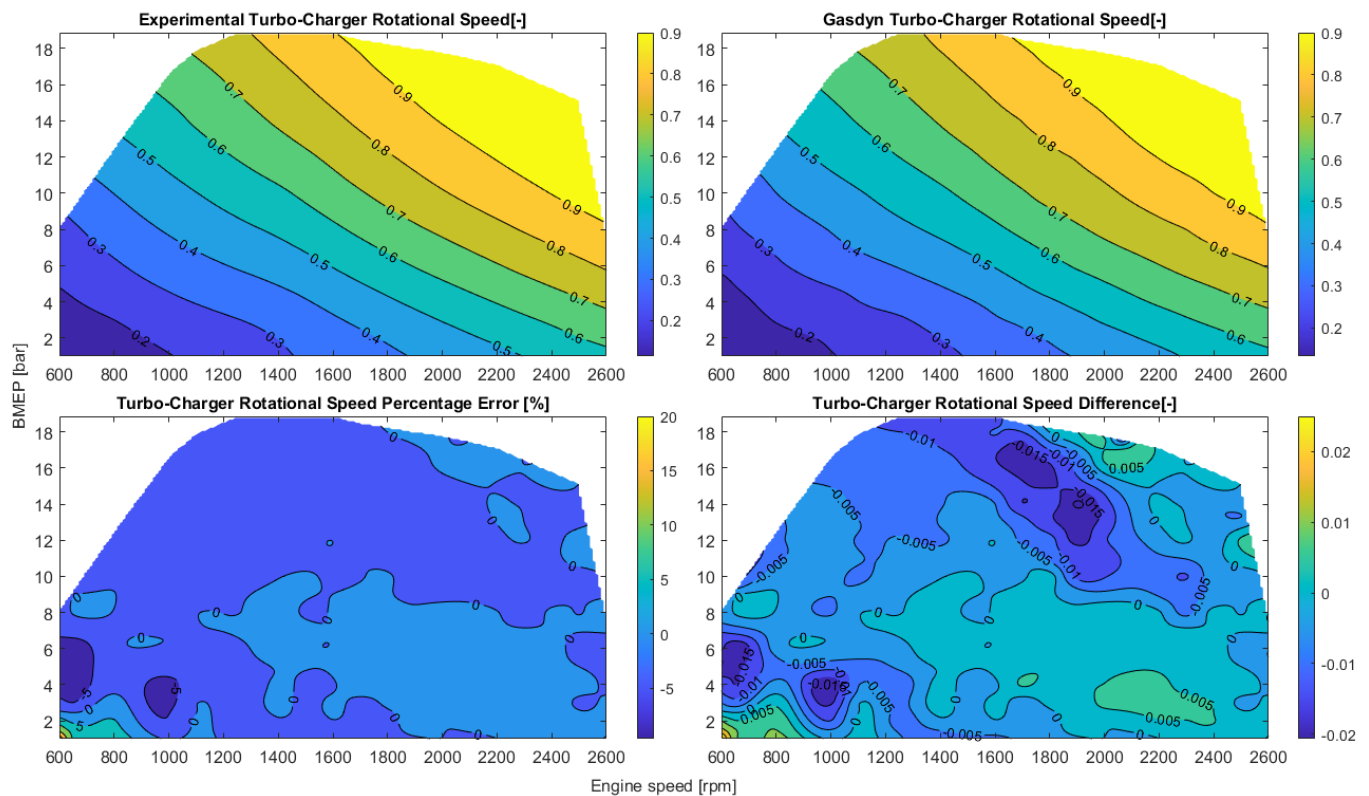
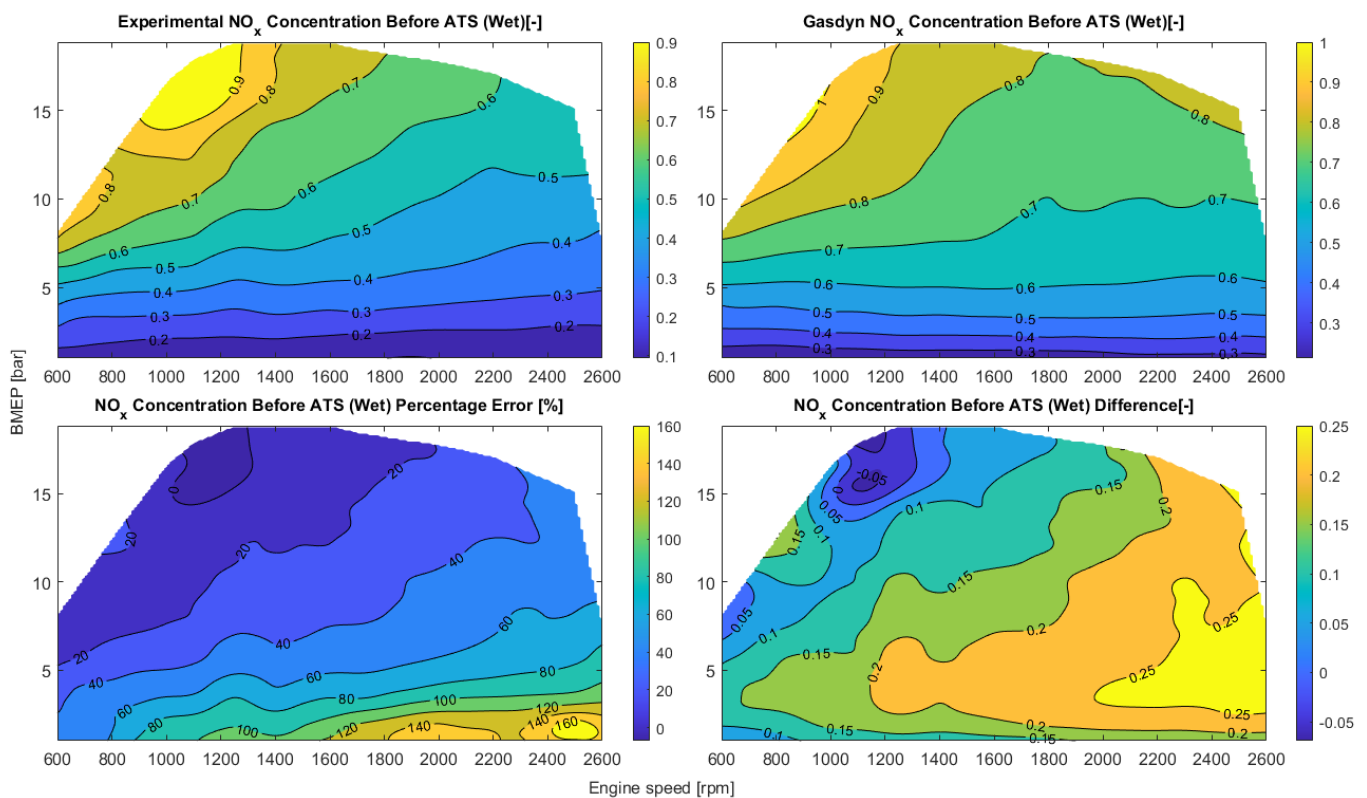


Figure A6. Contour plots of the measured and computed turbocharger rotational speed; relative and absolute errors on the whole steady engine map.



**Figure A7.** Contour plots of the measured and computed NO<sub>x</sub> concentration upstream of the ATS; relative and absolute errors on the whole steady engine map.

## Appendix B

This appendix contains the results regarding the transient validation of the 1D engine model, discussed in Section 3. The fuel consumption value is normalized with respect to the maximum value of the experimental data.

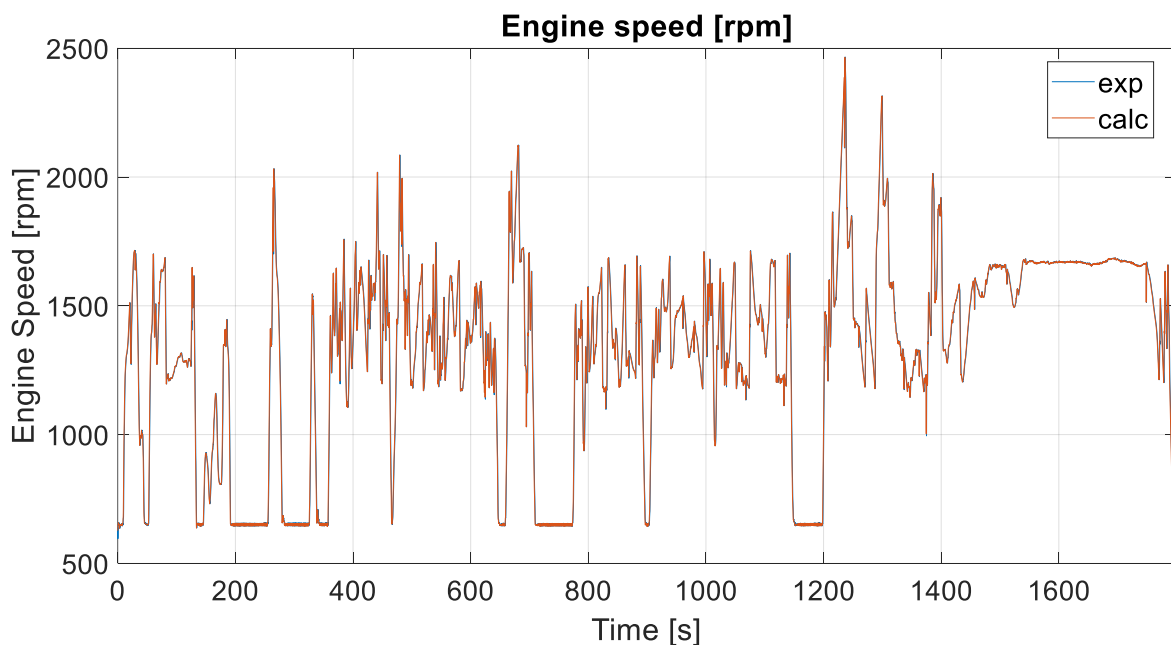


**Figure A8.** Engine speed during the simulated WHTC cycle.

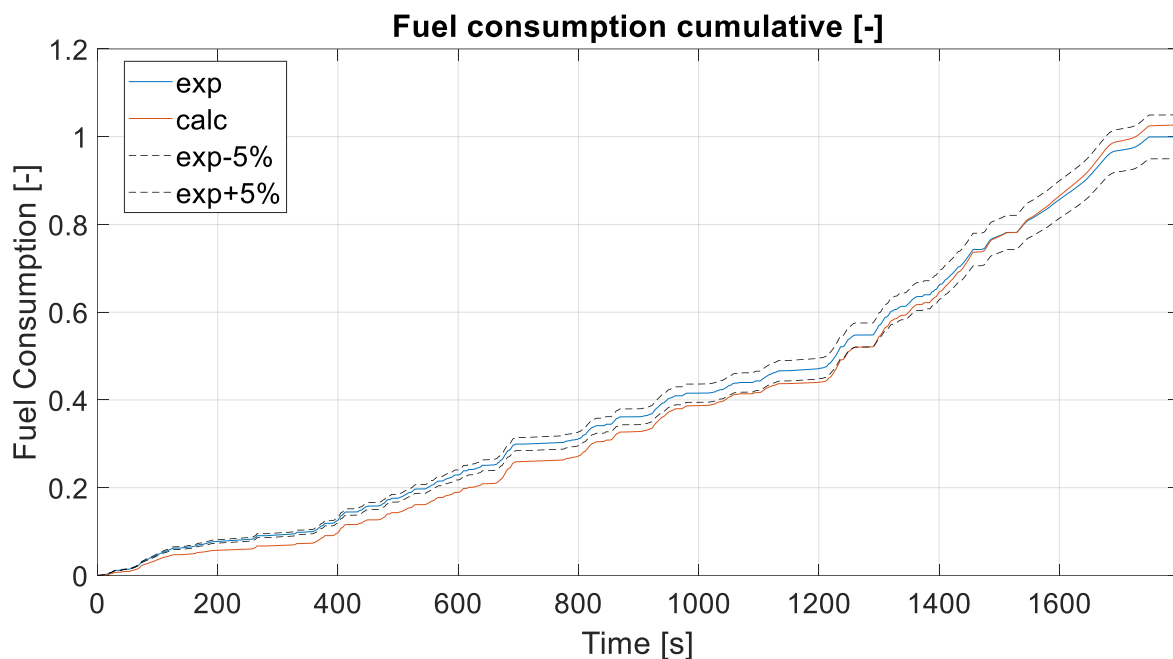


**Figure A9.** Normalized cumulative fuel consumption comparison with experimental data during the WHTC cycle.

## References

1. Grill, M.; Keskin, M.; Bargende, M. *Virtual RDE: Ensuring RDE Conformity of Hybridized Powertrains in the Early Stage of the Development Process*; VDI Berichte: Düsseldorf, Germany, 2020. [CrossRef]
2. Olmeda, P.; Martín, J.; Arnau, F.J.; Artham, S. Analysis of the energy balance during World harmonized Light vehicles Test Cycle in warmed and cold conditions using a Virtual Engine. *Int. J. Engine Res.* **2020**, *21*, 1037–1054. [CrossRef]
3. Finesso, R.; Spessa, E.; Venditti, M. Layout design and energetic analysis of a complex diesel parallel hybrid electric vehicle. *Appl. Energy* **2014**, *134*, 573–588. [CrossRef]
4. Mamikoglu, S.; Dahlander, P. *Modelling of Hybrid Electric Vehicle Powertrains—Factors That Impact Accuracy of CO<sub>2</sub> Emissions*; SAE Technical Papers; SAE International: Warrendale, PA, USA, 2019. [CrossRef]
5. Martínez, F.J.A.; Arnau, F.; Piqueras, P.; Auñón, A. *Development of an Integrated Virtual Engine Model to Simulate New Standard Testing Cycles*; SAE Technical Paper Series; SAE International: Warrendale, PA, USA, 2018. [CrossRef]
6. Millo, F.; Piano, A.; Zanelli, A.; Boccardo, G.; Rimondi, M.; Fuso, R. *Development of a Fully Physical Vehicle Model for Off-Line Powertrain Optimization: A Virtual Approach to Engine Calibration*; SAE Technical Paper; SAE International: Warrendale, PA, USA, 2021. [CrossRef]
7. Di Pierro, G.; Millo, F.; Scassa, M.; Perazzo, A. *An Integrated Methodology for OD Map-Based Powertrain Modelling Applied to a 48 V Mild-Hybrid Diesel Passenger Car*; SAE Technical Paper; SAE International: Warrendale, PA, USA, 2018. [CrossRef]
8. Heywood, J.B. *Internal Combustion Engines Fundamentals*; McGraw-Hill: New York, NY, USA, 1998.
9. Millo, F.; Giacominetto, P.F.; Bernardi, M.G. Analysis of different exhaust gas recirculation architectures for passenger car Diesel engines. *Appl. Energy* **2012**, *98*, 79–91. [CrossRef]
10. Ruoyang, Y.; Fletcher, T.; Ahmedov, A.; Kalantzis, N.; Pezouvanis, A.; Dutta, N.; Watson, A.; Ebrahimi, K. Modelling and Co-simulation of hybrid vehicles: A thermal management perspective. *Appl. Therm. Eng.* **2020**, *180*, 115883. [CrossRef]
11. Available online: <https://vision-xev.eu/> (accessed on 20 April 2023).
12. Liu, W. *Hybrid Electric Vehicle System Modeling and Control*; John Wiley & Sons: Hoboken, NJ, USA, 2017.
13. Vehicle Energy Consumption Calculation TOOl—VECTO. Available online: <https://europa.eu> (accessed on 20 April 2023).
14. Marinoni, A.; Tamborski, M.; Cerri, T.; Montenegro, G.; D’Errico, G.; Onorati, A.; Piatti, E.; Pisoni, E.E. 0D/1D Thermo-Fluid Dynamic Modeling Tools for the Simulation of Driving Cycles and the Optimization of IC Engine Performances and Emissions. *Appl. Sci.* **2021**, *11*, 8125. [CrossRef]
15. Marinoni, A.; Onorati, A.; Montenegro, G.; Sforza, L.; Cerri, T.; Olmeda, P.; Dreif, A. RDE cycle simulation by 0D/1D models to investigate IC engine performance and cylinder-out emissions. *Int. J. Engine Res.* **2022**. [CrossRef]
16. Usai, V.; Marelli, S. Steady State Experimental Characterization of a Twin Entry Turbine under Different Admission Conditions. *Energies* **2021**, *14*, 2228. [CrossRef]
17. Hadeif, J.E.; Colin, G.; Chamailard, Y.; Talon, V. Physical-Based Algorithms for Interpolation and Extrapolation of Turbocharger Data Maps. *SAE Int. J. Engines* **2012**, *5*, 363–378. [CrossRef]

18. Benson, R.S. *The Thermodynamics and Gas Dynamics of Internal Combustion Engines*; Clarendon Press: Oxford, UK, 1982; Volume 1.
19. Onorati, A.; Montenegro, G. *1D and Multi-D Modeling Techniques for IC Engine Simulation*; SAE International: Warrendale, PA, USA, 2020.
20. Winterbone, D.; Pearson, R. Theory of Engine Manifold Design: Wave Action Methods for IC Engineers. *Appl. Mech.* **2001**, *54*, B109–B110. [[CrossRef](#)]
21. Gascón, L.; Corberán, J.M. Construction of Second-Order TVD Schemes for Nonhomogeneous Hyperbolic Conservation Laws. *J. Comput. Phys.* **2001**, *172*, 261–297. [[CrossRef](#)]
22. Corberán, J.M.; Gascón, M.L.L. TVD Schemes for the Calculation of Flow in Pipe of Variable Cross-Section. *Math. Comput. Model.* **1995**, *21*, 85–92. [[CrossRef](#)]
23. Montenegro, G.; Della Torre, A.; Onorati, A.; Fairbrother, R. A Nonlinear Quasi-3D Approach for the Modeling of Mufflers with Perforated Elements and Sound-Absorbing Material. *Adv. Acoust. Vib.* **2013**, *2013*, 546120. [[CrossRef](#)]
24. Montenegro, G.; Onorati, A.; Cerri, T.; Della Torre, A. *A Quasi-3D Model for the Simulation of the Unsteady Flows in I.C. Engine Pipe Systems*; SAE Technical Paper 2012-01-0675; SAE International: Warrendale, PA, USA, 2012. [[CrossRef](#)]
25. Serrano, J.R.; Arnau, F.J.; Piqueras, P.; Onorati, A.; Montenegro, G. 1D gas dynamic modelling of mass conservation in engine duct systems with thermal contact discontinuities. *Math. Comput. Model.* **2009**, *49*, 1078–1088. [[CrossRef](#)]
26. Bozza, F.; De Bellis, V.; Marelli, S.; Capobianco, M. 1D Simulation and Experimental Analysis of a Turbocharger Compressor for Automotive Engines under Unsteady Flow Conditions. *SAE Int. J. Engines* **2011**, *4*, 1365–1384. [[CrossRef](#)]
27. Broatch, A.; Novella, R.; Ricardo, G.T.; Jorge, G.S.; Pal, J.P. Investigation of the effects of turbulence modeling on the prediction of compression-ignition combustion unsteadiness. *Int. J. Engine Res.* **2021**, *23*, 541–559. [[CrossRef](#)]
28. Woschni, G. *A Universally Applicable Equation for the Instantaneous Heat Transfer Coefficient in the Internal Combustion Engine*; SAE Technical Paper 670931; SAE International: Warrendale, PA, USA, 1967. [[CrossRef](#)]
29. Liu, J.; Dumitrescu, C.E. Single and double Wiebe function combustion model for a heavy-duty diesel engine retrofitted to natural-gas spark-ignition. *Appl. Energy* **2019**, *248*, 95–103. [[CrossRef](#)]
30. Lavoie, G.A.; Heywood, J.B.; Keck, J.C. Experimental and Theoretical Study of Nitric Oxide Formation in Internal Combustion Engines. *Combust. Sci. Technol.* **1970**, *1*, 313–326. [[CrossRef](#)]
31. Maiboom, A.; Tauzia, X.; Hétet, J.-F. Influence of EGR unequal distribution from cylinder to cylinder on NO<sub>x</sub>–PM trade-off of a HSDI automotive Diesel engine. *Appl. Therm. Eng.* **2009**, *29*, 2043–2050. [[CrossRef](#)]
32. The Leading Standard to Exchange Dynamic Simulation Models. Available online: <https://fmi-standard.org/> (accessed on 20 April 2023).
33. Gamma Technologies Inc. *GT-SUITE User's Manual*; Gamma Technologies Inc.: Westmont, IL, USA, 2022.
34. Vukotic, M.M.; Mijavec, D.; Corovic, S. Electric machine and Inverter Coupled Multi-physical Models. In Proceedings of the 2021 IEEE Vehicle Power and Propulsion Conference (VPPC), Gijon, Spain, 25–28 October 2021. [[CrossRef](#)]
35. Pirooz, A.; Mierlo, V.; Maitane, B. 3D Thermal and 1D Electro-Thermal Model Coupling Framework for Lithium-Ion Battery Cells. In Proceedings of the 2021 IEEE Vehicle Power and Propulsion Conference (VPPC), Gijon, Spain, 25–28 October 2021. [[CrossRef](#)]

**Disclaimer/Publisher's Note:** The statements, opinions and data contained in all publications are solely those of the individual author(s) and contributor(s) and not of MDPI and/or the editor(s). MDPI and/or the editor(s) disclaim responsibility for any injury to people or property resulting from any ideas, methods, instructions or products referred to in the content.